Optimizing Hyperdamping Materials for Enhancing Vibration Control and Shock Attenuation Properties

Undergraduate Honors Thesis

Presented in Partial Fulfillment of the Requirements for Graduation with Distinction in the Department of Mechanical and Aerospace Engineering of The Ohio State University

By

Yu Song
Undergraduate Program in Mechanical Engineering
The Ohio State University

May 2017

Thesis Committee:
Ryan L. Harne, Advisor
Jason T. Dreyer

ABSTRACT

To reduce unwanted mechanical vibrations in automotive, aerospace, and civil engineering fields, recent research has investigated periodic metamaterials having especially architected topologies. Yet, these solutions employ heavy materials and narrowband, resonant phenomena which are unsuitable for the many applications where broadband frequency vibration energy is a concern and weight is a performance penalty. To overcome these limitations, a new idea for hyperdamping materials is recently being explored, such that improved vibration damping is achieved without the drawbacks of the conventional periodic metamaterials. On the other hand, optimized designs of hyperdamping materials have not been determined which suggests that best practices for design and implementation are needed. The objectives of this research are to identify optimized, architected topologies of hyperdamping materials having square cross-sections, and to study the roles of the significance of beam buckling and ability to reduce mass according to the porosity of the architected internal geometry. Through finite element simulations, new designs are evaluated to investigate the roles of geometric design and to guide the fabrication for testing. With impact experiments, it is seen that the tapered internal geometry design leads to a greater instantaneous acceleration amplitude immediately after impact while more rapidly attenuating the energy when compared to the solid elastomer mass. With shaker experiments, both the tapered and periodic voids designs show enhanced wave attenuation over broadband frequency ranges from 2 to 10 kHz when compared to the solid elastomer that is indeed heavier. The results show that square cross-section hyperdamping materials provide rapid suppression of broadband impact and wave energies in square-section structures that are utilized in numerous engineering applications.

ACKNOWLEDGEMENT

I first and foremost thank my advisor Prof. Ryan Harne. I would never accomplish this research over the past year without his patient instruction, kindly encouragement and constant support.

I also want to thank Prof. Jason T. Dreyer for his support and help as my committee member.

All related experiments in this research are conducted in the Laboratory of Sound and Vibration Research (LSVR) that is directed by Dr. Harne.

TABLE OF CONTENTS

LIST OF FIGURES

LIST OF TABLES

1 Introduction

1.1 Significance of Research

Unwanted mechanical vibrations are encountered throughout modern engineering disciplines including automotive, aerospace, marine, and civil applications. Examples of these vibrations can be found everywhere in engineering world. Vibrations transmitted as random or shock excitations through a car chassis due to road excitation sacrifice the comfort of passenger. Building oscillations resulting from pedestrian walking, running, or jumping inside the building and those result from machines mounted at roof exist in every building. [1]. Bridge oscillations caused by pedestrians, vehicles or wind can result in destruction of bridge. Existing of these unwanted mechanical vibrations perplexed engineers when design mechanical structures. Unique vibration control system needs to be designed each time to serve different purposes and conditions. An important way to reduce the detrimental effects of these vibrations is to dissipate the energy generated associated with them. By this vibration damping approach, the energy is prevented from doing harm to the engineering structure, from becoming annoying radiated noise, or from resulting in significant wear-and-tear on the structural system.

1.2 Review of Previous Research

Researchers have recently investigated periodic metamaterials based on elastomer material systems with cellular topologies for the purpose of enhancing wave and vibration energy damping and trapping. Resonance-based metamaterials leverage mass-spring effects to yield large tuned vibration absorption. The periodic and elastic metamaterial absorb acoustic, wave and vibration energy by the transition among internal topology. For example, Shim et al. [2] arranged periodic monodisperse circular holes in two-dimensional elastomer materials to adjust the wave energy attenuation properties of the architectures. Wang et al. [3] reported a metamaterial whose response is controlled by mechanical deformation with elastomeric coating and easy-to-buckle elastic beams. Nouh et al. [4] considered a 2-D metamaterial plate-like configuration with periodic local resonances; this configuration was shown to provide narrowband vibration absorption when the plate was excited at one end. Baravelli and Ruzzene [5] investigated a lattice core within a beam frame so that tuned resonances would attenuated harmonic excitations of the frame. Florijin et al [6] and Rafsanjani et al [7] also investigated structures that successfully accomplish similar goals of vibration absorption and damping.

These advancements achieve vibration energy absorption for the respective applications, but each case shares similar limitations. Namely, the studies report the use of resonant phenomena which makes the systems operate in an inherently narrowband frequency and parameter-sensitive way; thus if adverse excitation energies change in frequency or characteristics, such resonant metamaterial concepts lose their effectiveness for vibration damping. In addition, the metamaterial usually involves dense material, such like silicone, or 3-D printed polymers, which limits their use in engineering applications where weight poses a great penalty. To overcome these problems, a lightweight material is required to provide broadband damping effect.

1.3 Hyperdamping Material Systems

An idea has recently been studied at the OSU Laboratory of Sound and Vibration Research (LSVR) where lightweight material systems are being engineered to provide broadband damping effects for vibration, acoustic, and impact energies. They are called hyperdamping materials. Experimentally, these materials reveal large reduction of force transmission through them as well as great acoustic energy absorption for noise control purposes [8]. As shown in Figure 1 (a), all hyperdamping material specimens are placed into metal tubes with inner diameter smaller than the specimen diameter to acquire strain. Figure 1 (b) shows how hyperdamping material achieve absorption of acoustic energy. Study of hyperdamping material also identified its capability in attenuation of impact. Intuitively, as shown in Figure 1(c) and (d), the comparison of dropping shells contain solid silicone mass and contain hyperdamping material is clear. Shell contains hyperdamping bounces lower than which contains solid mass, while the mass of hyperdamping material is even lower. Compared to existing metamaterials, hyperdamping material approach lower mass by minimizing the size and maximizing the damping effect. The principles of how it involving damping effect are discussed in Section 1.4. Because they do not leverage resonant phenomena to achieve their large energy absorption capability, they are not prone to the same limitations of the conventional resonant metamaterials.

Study of hyperdamping material has shown primary success. However, deeper studies are still required to broaden the usage of it. The primary design of hyperdamping material is in cylindrical shape, while square shape is also very common. Understanding of square shaped cross section hyperdamping material is still required.

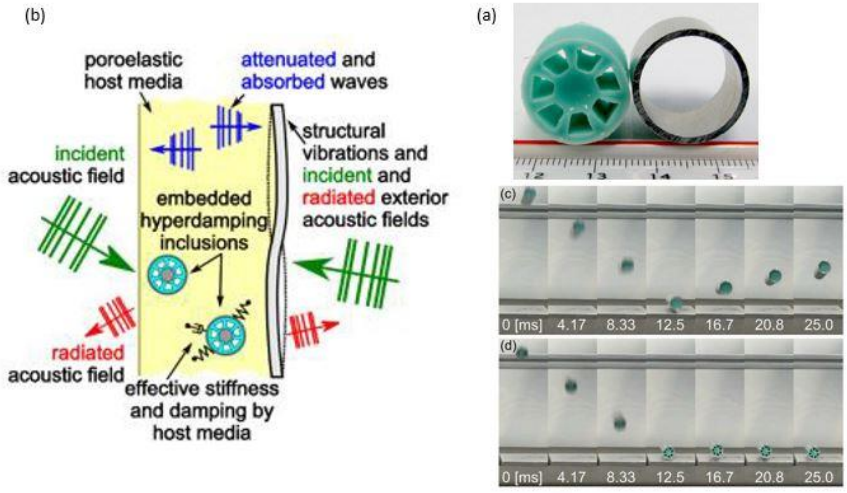

Figure 1:(a) Inclusion design principle that the elastomer element outer diameter is greater than the inner diameter of the rigid, metal shell. (b) Illustration of hyperdamping metamaterial with embedded inclusions in poroelastic media to attenuate and absorb incident acoustic waves and structural vibrations. [8] (c) video snap-shots when dropped from 471 [mm] with bulk elastomer and with (d) material inclusion. [9]

1.4 Buckling Structures and Energy Absorption

The concept of hyperdamping material relies on the buckling instability based phenomenon and cancelation of positive and negative stiffness [10]. The buckling phenomenon, also known as a case of elastic instability, means beams transfer through initial shape to a buckled shape with a significant sudden energy release [10] [11]. Negative stiffness can be approached in solid structure by transiting equilibrium states unstable [12] [13]. When the structure undergoes buckling, negative stiffness is instantaneously realized.

Now consider a buckling case. As shown in Figure 2 (a), a 1-D force is applied to beam. The load parameter p is defined proportioned to force P, where the point of $p = 1$ separates pre and post buckling. The damping ratio zeta is defined as equation

$$\varsigma = c / 2m\omega_n \quad \text{------ (1)}$$

where c is modal damping constant, m is mass and ω_n is the natural frequency. According to the equation, when natural frequency reaches zero at the critical point of $p = 1$, the damping ratio becomes infinite. Theoretically, structure should approach maximum damping at the critical buckling point [9].

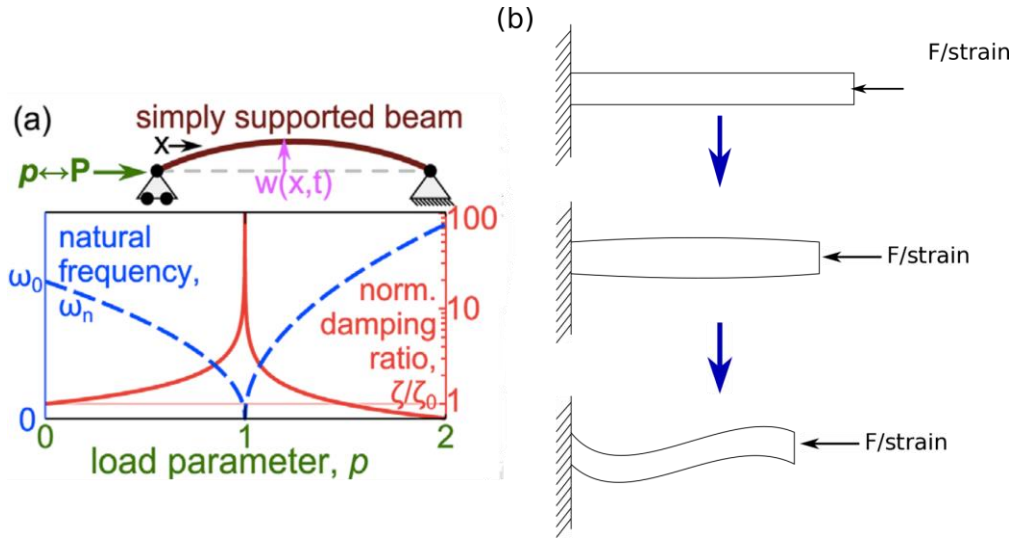

Figure 2: (a) Frequency and damping when beam buckled. [9] (b) Beam buckling when force or strain applied

1.5 Research Goal

With the explored and characterized preliminary design of hyperdamping materials, optimized designs can be determined. The preliminary design considered a circular cross-sectional topology, while square-shaped system cross-sections are also common throughout engineering structural systems. Examples include square shaped hollow structural section in building, square shaped structure in vehicle. As a result, the advancements provided by the new idea of hyperdamping materials have neither been optimized for circle geometric shapes nor have they been applied to the common square-shaped cross-sections for engineering design and optimization. Thus, the overall goal of this research is to create understanding for optimized design and utilization of hyperdamping materials that enable the significant attenuation of vibration, wave,

and shock energy that is required in numerous engineering applications. In this report, performance of square-shaped cross-section hyperdamping material will be evaluated with mechanical vibration and impact. Designed hyperdamping material aims to observe significant energy absorption of mechanical energy while undergoes vibration or impact. Research targets to show clues that topology designs have more or similar energy attenuated with lighter mass. As stated in Chapter 1.4, the topology design relies on the theory of vanishing natural frequency at nearly buckling point.

1.6 Overview of Thesis

This thesis is organized as follows. Chapter 2 discusses the finite element analysis model used to guide future experiments. Chapter 3 discusses the fabrication of specimens and experimental setup, include hammer impact test and shaker transducer test. Chapter 4 focuses on the results generated from the experiments, discusses significant experimental trends, and provides deeper insights of hyperdamping material. Chapter 5 recalls significant experimental results and provide future research opportunities.

2 Geometry Designs and FEA model

In Chapter 2, design process of two hyperdamping models is stated. Interested parameters of each model are given in Chapter 2.2. The model is then evaluated in FEA (Finite Element Analysis) modeling to guide fabrication of specimens. The modeling process and results are presented in Chapter 2.3 and Chapter 2.4.

2.1 Beam Study and Design Constraints

Elastomer beams work as springs [14]. The hyperdamping material can be considered as tuned mass damper, while the inner mass can be considered as a small mass connected to the original mass through springs. According to previous studies, structures loaded near the point of buckling exhibit an infinitely increasing damping ratio due to the vanishing natural frequency [2]. Thus, the design feature of the hyperdamping material is a set elastomer beams that connect to small mass, with the beams are able to approach buckling when strain applied to the structure. It requires beam undergoing normal load as shown in Figure 2 (b) when the cross-section of the whole structure shrink.

In the design, some parameters are defined to have the geometry changeable. Later experiment will study roles of these parameters to understand under what condition the hyperdamping material could achieve better performance in energy absorption. According to theory stated in last paragraph, interested parameters are those relate to the buckling status of the beams.

Before starting this research, to find the relationship between beam geometry and beam buckling, a 2-D elastomeric beam is studied in finite element model. Results shows longer and thinner beam requires lower strain to buckle. Thus, in the hyperdamping design, parameters can change the ratio of beams thickness and length, and parameters can change strain value should be selected to study.

2.2 Geometry Designs

Based on the theory stated above [14], two geometries as shown in Figure 3 are investigated. Each of them allowed beams to buckle when strain was applied uniformly on four sides. Three parameters were selected to study for each design. As study of cylindrical-shaped design, the specimens are placed into metal tube to approach strain. The tube side length should be smaller than the specimen side length. The metal tube was used in later experiment has inner side length of 0.0159m (0.625in). Details of how specimens are prepared will be described in Chapter 3.

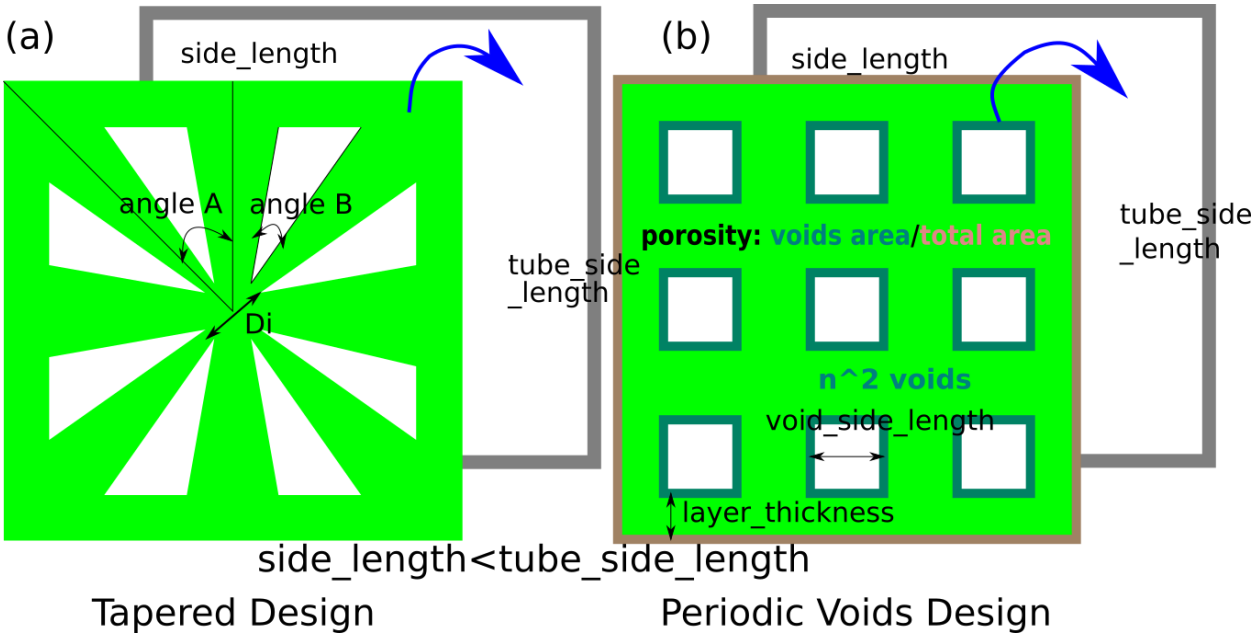

Figure 3: (a) Geometry and parameters of tapered design. (b) Geometry and parameters of periodic voids design

As shown in Figure 3(a), the first design called tapered design. It was inspired by previous cylindrical design studied in LSVR. It has shown that geometry with radially arranged beams could satisfy requirements of hyperdamping material. With this design, the square is divided into four radially symmetry parts, result in eight tapered beams being arranged radially around the inner mass. The strain applied is changed by changing the side length of the specimen, with the tube side length as constant. The design is divided into eight identical parts by diagonal, horizontal and vertical lines. Each part has a 45º central angle, and it is defined as angle A. Angle B is defined as the inner angle of the void triangle, as labeled in Figure 3(a). The inner vertexes of the void triangles are arranged on a circle centered at the geometry center. The diameter of the circle is called inner mass diameters (Di).

Beams in this design are tapered, so that they do not have uniform thickness. However, parameters stated above can vary the thickness generally. For ease of study, all interested parameters are defined as ratios. They are open angle ratio ($angle\ B/angle\ A$), inner mass diameter ratio ($D_i/side\ length$) and strain ($(side\ length - tube\ side\ length)/tube\ side\ length$). The change in open angle ratio (B/A) affects the mass of specimen, as well as the thickness and tapering of radially arrayed beams. The ratio of Di/side is the ratio between the inner mass diameter and the side length. Change in the inner mass diameter ratio influences the length of the beams and the mass of the specimen. Other constants and variables involved while define the geometry are listed in Table 1.

Table 1: Parameters in Tapered Design

Constants		
Variable Name	Value	Unit
$tube\ side\ length$	0.015875	[m]
angle A	0.78540	[rad]
Variables Related to Parameters		
angle B	$B/A * \text{angle A}$	[rad]
$side\ length$	$\text{strain} * \text{tube\_side\_length}$	[m]
$inner\ mass\ diameter$	$Di/side * \text{side\_length}$	[m]
$layer\ thickness$	$0.22 * \text{side\_length}$	[m]

The second design, with geometry shown in Figure 3 (b), called periodic voids design. Square shaped voids are arranged periodically on the cross section. The geometry is defined in this way to emphasize the existing of beams. When the specimen placed in smaller metal tubes, strain is applied uniformly normal to four sides of the square cross-section. Horizontal and vertical beams will both experience axial strain.

Similarly, the strain is studied by changing the side length. Each cross section contains n^2 voids in total. The total area of the voids is defined as a ratio of area of cross section, called porosity. Visually, in Figure 3 (b), sum of area of squares boxed with dark green is the total voids area, while the area big square boxed with light red is the area of cross section. Both number of the voids (n^2) and the porosity can change the length and thickness of beams. Other involved constants and variables are listed in Table 2 and labeled in Figure 3 (b).

Table 2: Parameters in Periodic Voids Design

Constants		
Variable Name	Value	Unit
tube side length	0.015875	[m]
Variables Related to Parameters		
side length	$\text{strain} * \text{tube\_side\_length}$	[m]
layer thickness	$0.22 * \text{side\_length}$	[m]
total void area	$\text{porosity} * (\text{side\_length} - 2 * \text{layer\_thickness})^2$	$[m^2]$
void side length	$\sqrt{\text{total\_void\_area}/n^2}$	[m]

2.3 COMSOL Multiphysics and Model Setup

A finite element model is created of the specimens to study the influences of design parameters and to guide future fabrication for experiments. The finite element method is a computer-based numerical method to solve engineering problems and mathematical physics problems. [15] The area of this research is structural mechanics. The software used is COMSOL Multiphysics. For each design, the model is defined into a Prestressed-Eigenfrequency study, which is a build-in solver in COMSOL software. The study will return the damped or undamped eigenfrequencies and mode shapes of a structure.

The model is defined in 2-D plane, while the length (thickness, perpendicular to plane) of it being considered as 1m. The geometry is defined in parameters as shown in Table 1 and Table 2.

The material is used in fabrication is silicone rubber. The material properties are defined as shown in Table 3. The material properties are determined empirically using the silicone rubber ultimately employed for specimen fabrications in the laboratory. Details of material, like brand, type, etc. are given in Chapter 3.

Table 3: Silicone Rubber Material Property

Material Property	Value	Unit
Young's Modulus	7.52E+05	[Pa]
Density	1145	$[kg/m^3]$
Possion Ratio	0.49	N/A

Table 4: Parametric Analysis Sweep Range

Variable Name	Sweep Range	Unit
Tapered Design		
Open Angle Ratio (B/A)	[0.7,1]	N/A
Di/side_length	[0.16, 0.3]	N/A
side_length	$tube\ side\ length * [1.02, 1.05]$	[m]
Periodic Voids Design		
voids number, n	[3,4,5]	N/A
porosity	[0.274,0.395]	N/A
side_length	$tube\ side\ length * [1.04, 1.07]$	[m]

After defining the geometry and material properties, other features and physics of the model are defined in following steps:

- The physics Prescribed Displacement is defined on boundaries. As shown in Figure 4, the left and bottom sides are fixed by define the displacement as zero. Strain is applied by define negative displacements on right and top sides. The value of the displacement is the difference between tube side length and model side length.
- Free Triangular meshes are defined through the geometry uniformly. The mesh density is visually shown in Figure 4 (b). The maximum mesh element size is defined as $side\ length/50$, which means 50 mesh elements are defined at each side. Finer mesh can result in more accurate result. However, more mesh can cause the model extremely time consuming. To balance the time cost and data accuracy, after trying several times to compare results from different mesh definitions, above setting is determined. Figure shows visual of tapered design, and periodic voids design is defined in the same way.
- For each design, parametric analysis is evaluated with three interested parameters (discussed in Chapter 2.2). A parametric analysis can find solution dependence due to variation of a specific parameter. Visual difference while changing each parameter is shown in Figure 5. Besides them, another parameter will be swept is side length (strain). The 3-D printer for future fabrication has resolution about 0.125mm. Previous attempts show that the thinnest wall can be printed is about 1mm. The range of each parameter is decided based on that no wall will have thickness lower than 1mm when parameters are in extreme value. The ranges are shown in Table 4. Except the voids number in periodic voids design, each parameter has 17 points evaluated in the range. In each evaluation, two parameters are changing while one parameter is controlled to a specific value.

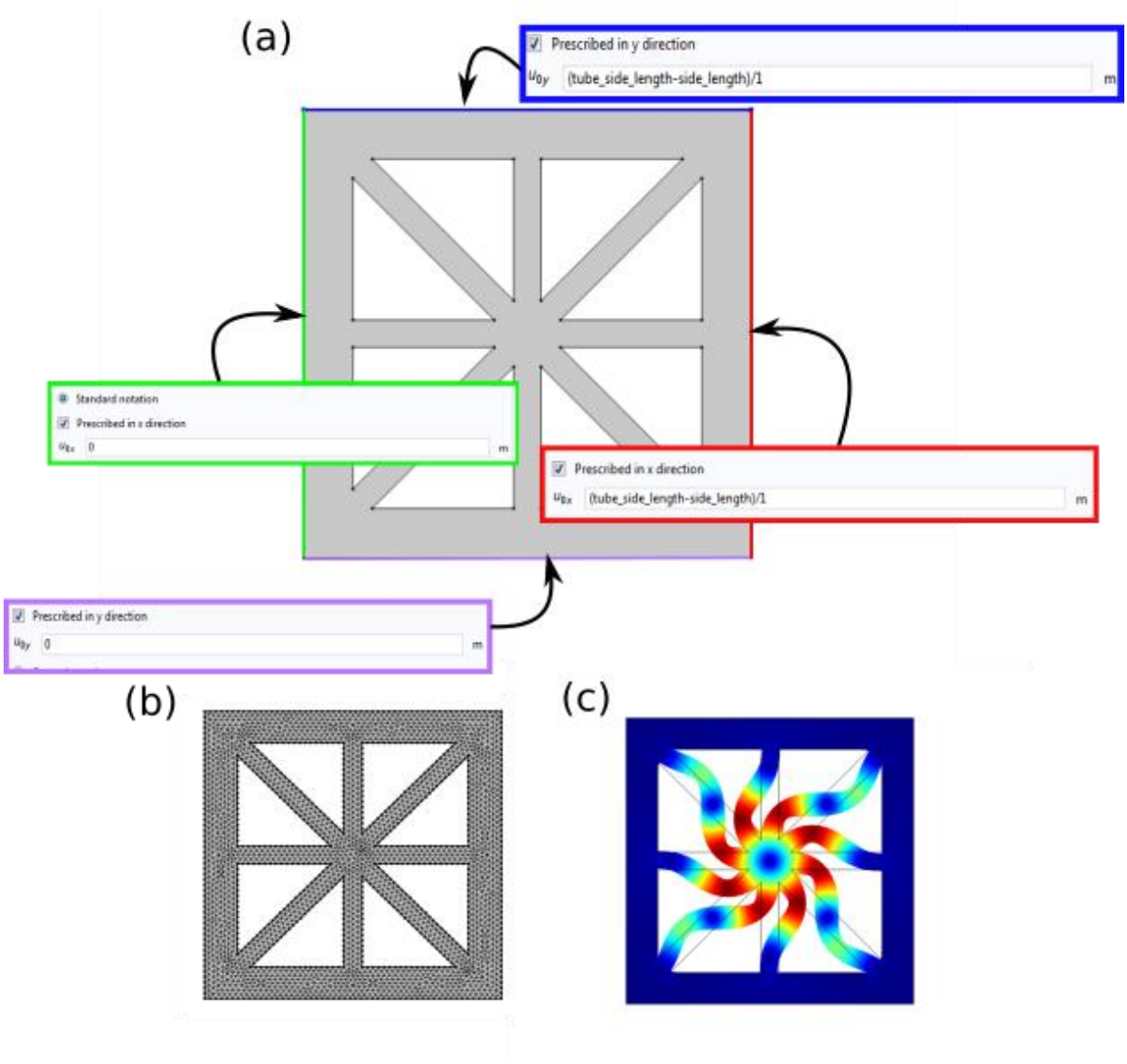

Figure 4: Finite Element Model Setup and Graphic Result. (a) Prescribed displacement on each side. (b) Mesh density. (c) Solved Mode Shape

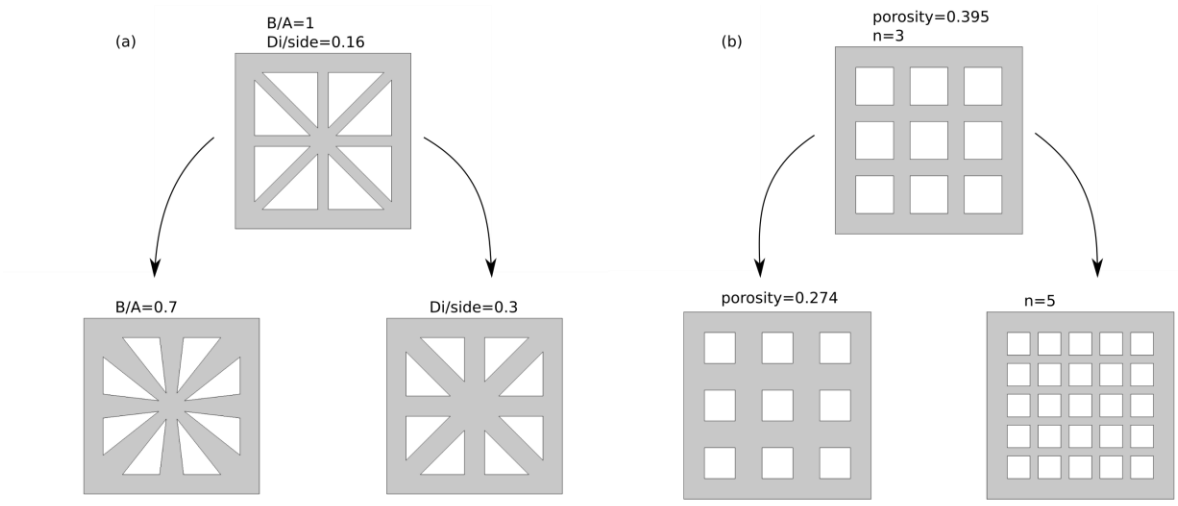

Figure 5: Visual Change when Changing Each Parameter for (a) Tapered Design. (b) Periodic Voids Design.

2.4 Modeling Result

The fundamental eigenfrequency of the hyperdamping material architecture subjected to given constraints and according to certain design parameters is plotted in Figure 6. The contour plot reveals areas of high and low fundamental eigenfrequency by the color shading, with high value of eigenfrequency indicated by brighter colors closer to yellow. Dark blue colors on the contours indicate post-buckled configurations since the fundamental eigenfrequency vanishes in (real) absolute value. Thus, the line between the dark blue and light blue is the line of critical buckling. The idea of selecting parameter combinations for future fabrication is to select some not buckled, some critical buckled, some post buckled. And the roles of parameters can be studied.

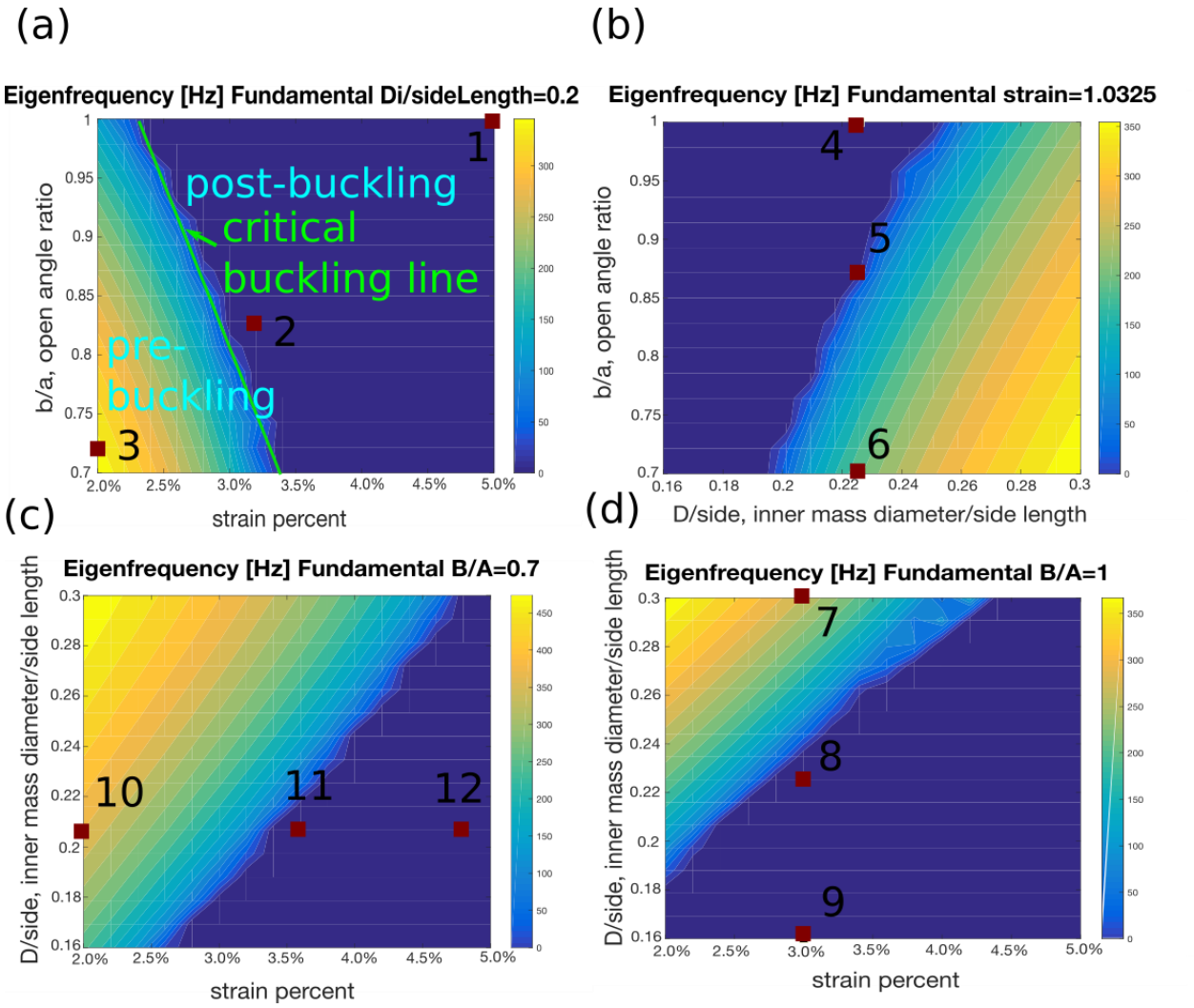

Figure 6: Contour plots of results of finite element model for tapered design with (a) strain and open angle ratio changing, and Di/side controlled to 0.2. (b) Di/side and open angle ratio changing, and strain controlled to 3.25%. (c) strain and Di/side changing, and open angle ratio controlled to 0.7. (d) strain and Di/side changing, and open angle ratio controlled to 1.

Figure 6 shows results from tapered design modeling. In Figure 6 (a), the plot shows result with Di/side controlled to 0.2. In this plot, it is observed that dark blue color with zero real eigenfrequency lies at higher strain and higher open angle ratios. Namely, specimens with higher strain and higher open angle ratio would be buckled. In this plot, three parameter combinations are selected. They lie most likely perpendicular to the critical buckling line. They are specimens from 1 to 3 in Table 5. Exact value of each parameter is also listed in the table. Since specimen 1 and specimen 3 are far away the critical buckling line, they are more obvious in respectively post-buckling and pre-buckling status.

In Figure 6 (b), eigenfrequency varies with Di/side and open angle ratio, with strain is controlled as 3.25%. Zero eigenfrequency values lie at lower Di/side and higher open angle ratio. In the other word, low Di/side and high open angle ratio cause structure buckling. The parameter combinations are selected to emphasize

the study of role of open angle ratio. By selecting them vertically in the plot, three different open angle ratio values are taken with strain and Di/side the same. They are specimens 4 to 6 in Table 5.

In Figure 6 (c), parameters Di/side and strain are swept with open angle ratio controlled at 0.7. In Figure 6 (d), same parameters are swept with open angle ratio controlled to 1. With x and y axis are both in same range, larger dark blue area in figure (d) highlighted that larger open angle ratio promotes buckling. The trend in both plots, that dark blue lies at higher strain and lower Di/side, shows higher strain and lower Di/side easily to approach buckling. In figure (c), three specimens are selected horizontally to study the role of strain. And in figure (d), they are selected vertically to study the role of Di/side.

In all, mapping of these plots show that post-buckling design usually has larger open angle ratio, smaller Di/side and larger strain. With twelve parameter combinations selected in Figure 6, role of three parameters, open angle ratio, Di/side and strain, can be studied in future experiment. As well, the effect of buckling status can also be clearly compared.

Table 5: Selected Parameter Combinations for Tapered Design

Specimen #	Strain percent	B/A, open angle ratio	Di/side length
1	5.00%	1.00000	0.20000
2	3.20%	0.82857	0.20000
3	2.00%	0.72143	0.20000
4	3.25%	1.00000	0.22588
5	3.25%	0.87143	0.22588
6	3.25%	0.70000	0.22588
7	3.20%	1.00000	0.30000
8	3.20%	1.00000	0.22533
9	3.20%	1.00000	0.16000
10	2.00%	0.70000	0.20667
11	3.60%	0.70000	0.20667
12	4.80%	0.70000	0.20667

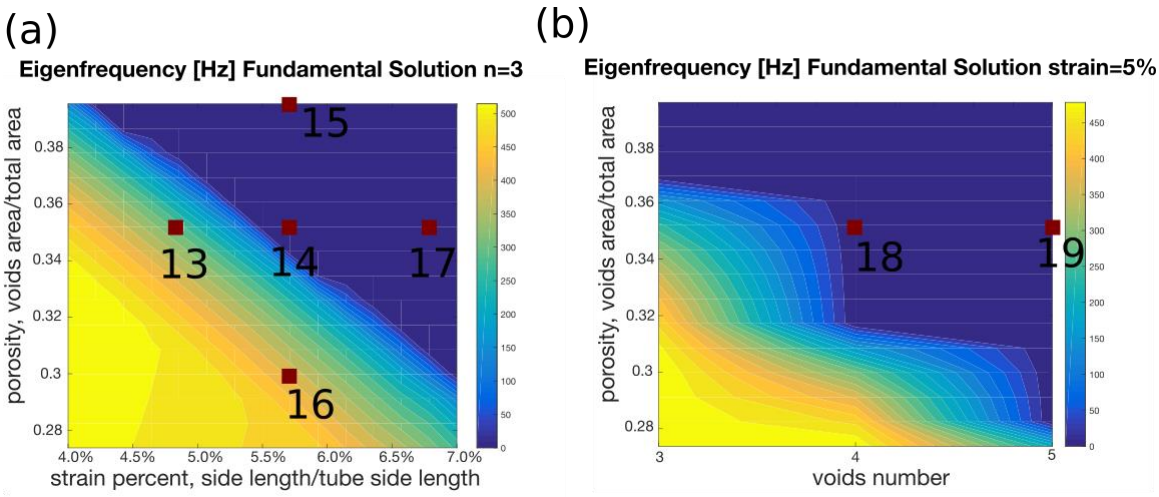

Figure 7: (a) Contour plots of results of finite element model for periodic voids design with (a) porosity and strain changing, and n controlled to 3. (b) porosity and n changing, and strain controlled to 5%.

Figure 7 mainly shows modeling results for periodic voids design. In figure (a), the voids number is controlled to three. With porosity increasing and strain increasing, structure more easily approach buckling. Five parameter combinations are selected from this figure. Specimen 13, 14, 17 are in comparison of strain. Specimen 16, 14, and 15 are in study of role of porosity.

Figure 7 (b) shows the critical buckling line is in steps due to the integer nature of the voids number parameter. The figure only help in selection of specimen. Specimen 18 and 19 are selected with different voids number. Combine specimen 14 and 18, 19, the role of voids number is studied with the strain and porosity unchanging.

Overall, specimen with higher strain and higher porosity tend to be easier to buckle according to the FE model results. Seven specimens are selected for future test, by which the roles of porosity, voids number and strain are studied as described in Table 6.

Table 6: Selected Parameter Combinations for Periodic Voids Design

Specimen #	Strain percent	Porosity	Voids number, n
13	4.8571%	0.35200	3
14	5.7143%	0.35200	3
15	5.7143%	0.39546	3
16	5.7143%	0.29985	3
17	6.7857%	0.35200	3
18	5.0000%	0.35200	4
19	5.0000%	0.35200	5

3 Experimental Method

In this chapter, the fabrication process and size measurement of specimens are discussed in first section. Then, setup for two experimental tests and data acquisition system are described.

3.1 Specimen Fabrication

To fabricate specimens, molds are firstly 3-D printed by FlashForge Creator Pro 3D printer with ABS plastic. The mold contains two parts, a square shaped shell (Figure 8 (c)) and a base (Figure 8 (a) and (b)) with the shape of voids are printed. The ribs designed on the base are used to align the shell. Approximate 0.25mm clearance is given on each side for assembling. The inner side length of shell is oversized in SolidWorks to overcome the printing error. Attempts show about 2% oversizing is required. Two mold parts are bonded together (Figure 8 (d)) with wax and well-mixed silicone rubber liquid is poured into the mold. The type of silicone rubber is Mold Star 15S by Smooth-On. After the silicone rubber is cured, the specimens are de-molded and cut to identical lengths. Then, all specimens are washed by cold water to remove wax. Besides selected specimens as discussed in Chapter 2, a pure solid mass is fabricated as control group and labeled as specimen 20.

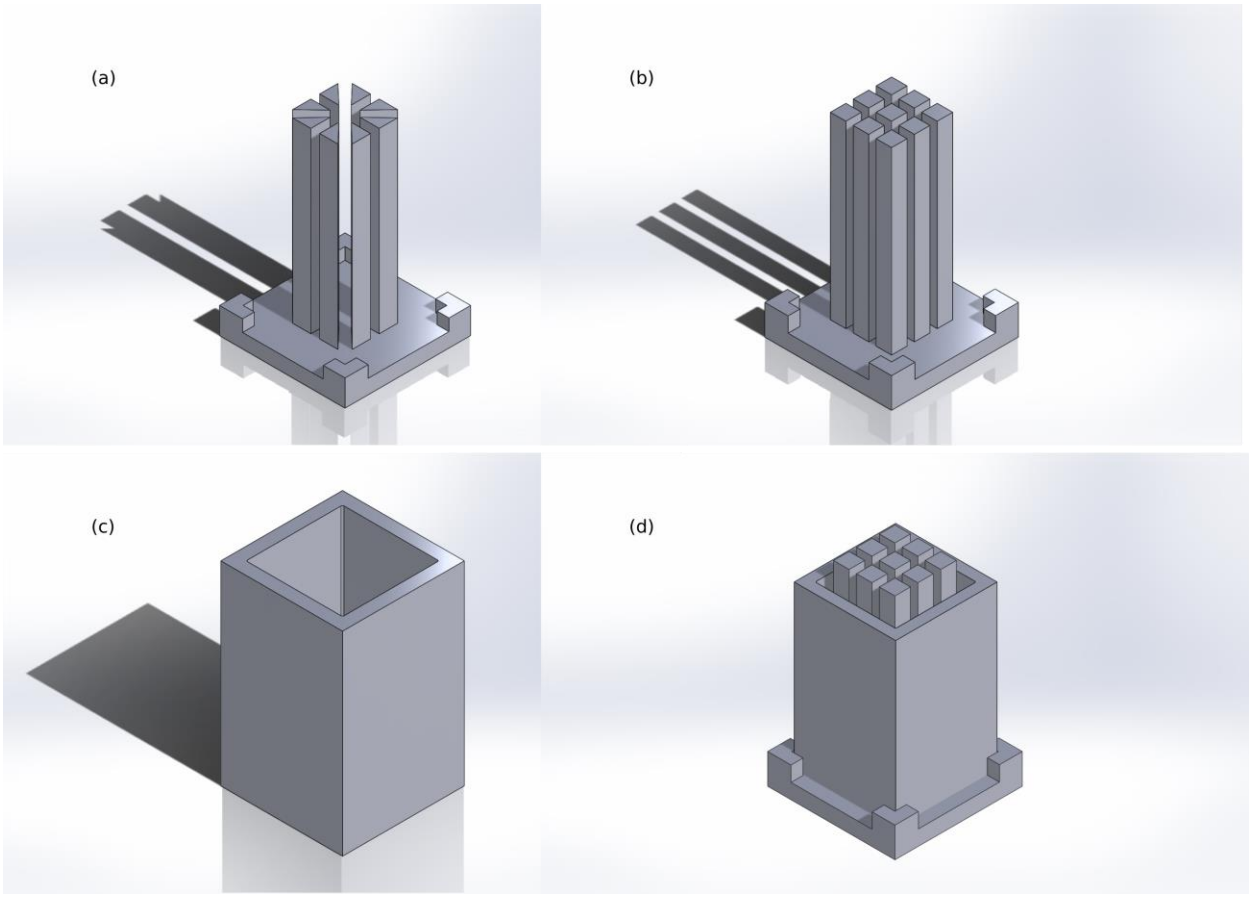

Figure 8: CAD screen shot of (a) tapered design base mold. (b) periodic voids design base mold. (c) shell mold. (d) assemble of base and shell.

After demolding and cleaning, specimens are measured. The measured specimen dimensions are given in Table 7. The side length of each specimens is measured and then calculated to strain. The length of the specimen is the thickness perpendicular to the cross-section. Molds are designed into 0.03429m. The target length is 0.03048m after cutting. The weights of specimens are measured in grams. Hyperdamping specimens have mass from 5.5g to 8g, while the control specimen has weight about 9g. The weight of specimen results both from cross-section geometry design and specimen length. To have a more direct comparison, the length density is defined as $length\ density = mass/length$. The average of length density of hyperdamping material specimens is 219g/m, while it is 305g/m for control specimen. With same length, hyperdamping specimens involves overall 28% less mass than control specimen does.

Table 7: Fabricated Specimen Measurement

Specimen #	Designed Strain	Measured Strain (%)	Strain Error (%)	length (m)	mass(g)	Mass/unit length(g/m)
1	5.00%	4.16%	16.80%	0.03160	6.317	200
2	3.20%	3.28%	2.50%	0.03139	6.943	221
3	2.00%	1.84%	8.00%	0.03313	7.470	225
4	3.25%	3.28%	0.92%	0.03340	6.877	206
5	3.25%	3.44%	5.85%	0.03233	7.233	224
6	3.25%	2.96%	8.92%	0.03207	7.898	246
7	3.20%	2.96%	7.50%	0.03181	7.127	224
8	3.20%	3.52%	10.00%	0.03316	6.869	207
9	3.20%	3.52%	10.00%	0.03166	5.682	179
10	2.00%	2.24%	12.00%	0.03194	7.557	237
11	3.60%	3.76%	4.44%	0.03287	8.191	249
12	4.80%	5.04%	5.00%	0.03244	7.887	243
13	4.8571%	3.92%	19.29%	0.02957	6.895	233
14	5.7143%	5.36%	6.20%	0.03185	6.534	205
15	5.7143%	4.64%	18.80%	0.03120	6.113	196
16	5.7143%	5.12%	10.40%	0.03071	7.384	240
17	6.7857%	4.56%	32.80%	0.03192	6.803	213
18	5.0000%	3.52%	29.60%	0.03162	6.187	196

19	5.0000%	3.28%	34.40%	0.03010	6.557	218
20	0.0000%	0.00%	0.00%	0.02935	8.953	305

All specimens are placed into aluminum tube to apply strain. A flat-head tweeze is used for assembling. For tapered design, the inner mass is rotated and pulled by the tweezer to assemble the specimen into metal tube. For periodic voids design, the specimen is placed into the tube by hand. Tweezer is then used to adjust the specimen to make sure it is at proper position. The wall of specimens cannot be curved. The type is 6063 aluminum rectangular tube, obtained from McMaster-Carr, with outside side length of 0.0192m (3/4 in) and wall thickness of 0.016m (1/8 in). The tubes are cut into 0.03048m (1.2 in) lengths, and the edges are polished. All tubes are washed by cold water and quickly dried up to remove metal scraps that may tear the silicone rubber specimens. Specific machining steps for each testing is described in Chapter 3.2 and Chapter 3.3.

3.2 Hammer Impact Testing

The tapered design and control group are tested in hammer impact testing. All experiments are conducted on SMART TABLE UT2 isolation table. As shown in Figure 9, the specimen is suspended on a fixed frame by fishing line. The fishing line are threaded through the specimen from the center of inner mass guided by needle. The fishing line is then tight on the frame with screw and washer on each side. The fishing line should be tight enough to allow the specimen oscillation.

To thread through the specimen with fishing line, a needle is required to thread through the specimen first. Push the needle until only the hole is out of the specimen. Then, the fishing line is passed through the hole on the needle. Pull the needle from the other way until both the needle and fishing line is thread through. Remove the needle and directly pull the fishing line until the outside length is enough to suspend the specimen on the frame.

Two accelerometers (PCB U352A10) are attached on the specimen via wax from back and bottom. Accelerations of the specimen on both axis can be measured. The force impact hammer (PCB 086C01) is used to apply impact. As shown in Figure 9, the impact should be applied to the specimen from the edge with the direction as shown with red arrow. The impact position is assured by observing all traces caused by impact in similar position on the edge. Thus, two accelerometers can be excited equally. One impact is applied every two seconds. 100 impacts is applied and measured in total for each specimen. The impacts are distributed uniformly in a range of force value, which is from <50N to about 300N in practice. To achieve uniform distribution, first one third impact should be applied with slight force; second one third should be with harder force; last one third should be with very hard force. Practice is required to make sure the accelerometers are excited properly and impact forces are distributed properly. After one hit, after specimen oscillates for about one second, it is necessary to stop it by hand before next hit.

The specimens are replaced by removing the fishing line from the frame each time. When operate the experiment, to assure the setup is identical for every specimen, one side (left in the figure) is tighten on the

frame by bolt first. Then, the other side is tighten by hand before fasten the bolt. The specimen is excited by hand to assure similar oscillation is observed each time before start testing.

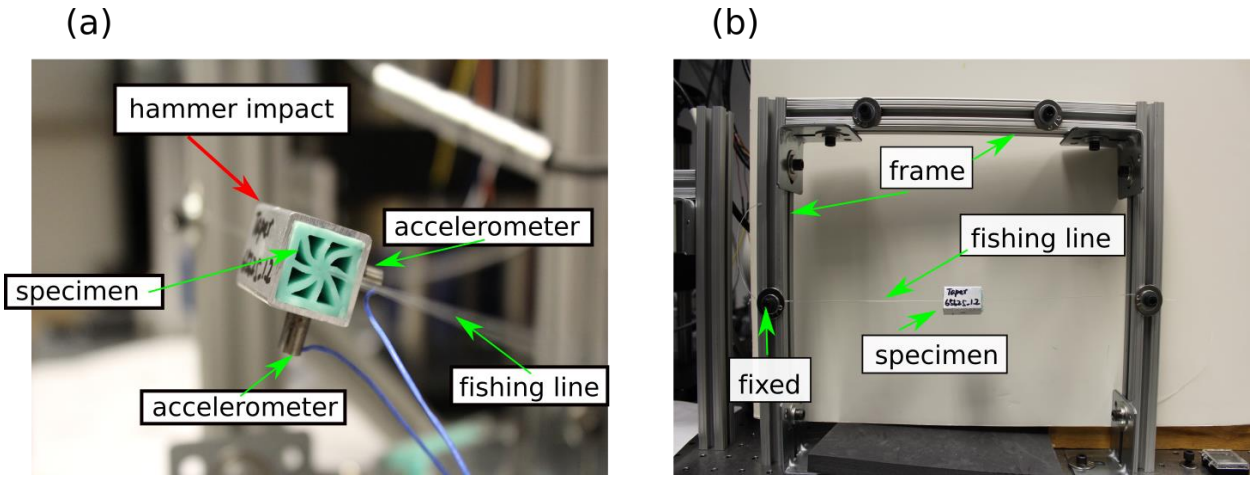

Figure 9: Hammer Impact Testing Setup (a) side view (b) front view

3.3 Shaker Testing

All specimens undergo shaker testing. This testing setup is also constructed on SMART TABLE UT2 isolation table. A force transducer (PCB 208C01) is mounted between specimen and shaker. A metal tube is threaded with a 10-32 hole to mount on the force transducer. An accelerometer (PCB 352A24) is attached on the top of specimen via wax. The input force exciting the specimen and output acceleration that the specimen undergoes are measured.

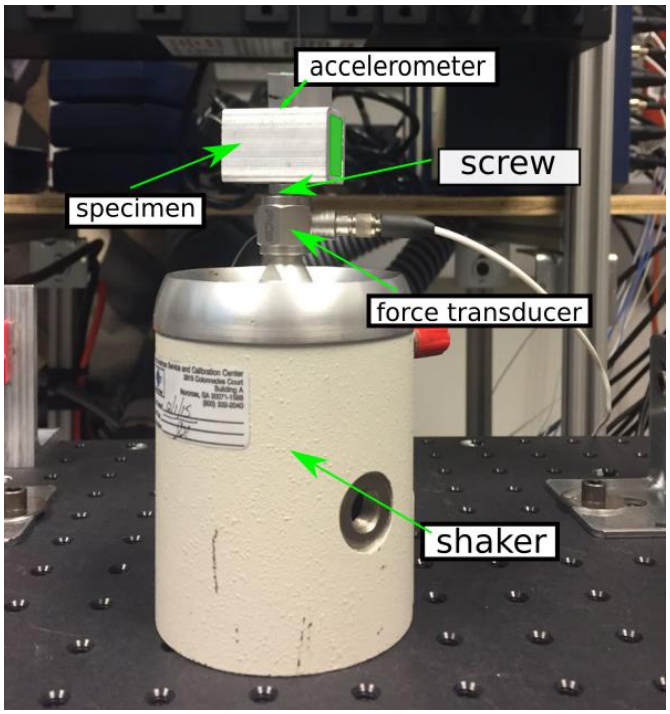

Figure 10: Shaker Testing Setup

3.4 Data Acquisition System

Signal conditioner output is wired into NI SCB-68A, which is connected to a NI PXIe-6368 card. The data acquisition card is fed to a NI PXIe-1073 DAQ system. The DAQ system is then connected into HP Z210 Workstation PC running Windows 7. Data is collected by MATLAB version R2016b.

Sample data acquisition code is attached in appendix. In Chapter 6.1.2, the data acquisition file for hammer impact test is given. The sampling frequency is 131,072Hz. The data is filtered from 50 Hz to 18000 Hz. Data out of this range is considered as noise. Measured voltage of each sensor is multiplied by its sensitivity to convert to force or acceleration. The sensitivity of the transducer on the hammer is 1/0.01108 N/V. The sensitivities for two accelerometers are respectively 14.06 ($\frac{m}{s^2}/V$) and 16.96 ($\frac{m}{s^2}/V$). The sensitivities are calibrated before testing. After transfer voltage signal to force, value above 10N is considered as an impact. 0.05s data is collected after each impact. Results are presented in both frequency and time domain. Calculation is given in Chapter 4.

In Chapter 6.1.3, MATLAB file for shaker transducer test data acquisition is provided. The data is filtered in 500 Hz to 20,000 Hz. Data outside this range is cut off for calculation. The sampling frequency is 131,072Hz. Each test will run 60s, while all data inside this 60s is recorded. Input force and output acceleration is computed by multiply the voltage signal with sensitivities. The sensitivity of the transducer is 1/0.1125 N/V. The sensitivity of the accelerometer is 1/0.011022 ($\frac{m}{s^2}/V$). Data is presented in frequency domain, related calculations are given in Chapter 4.

Workspace is auto saved with file name include specimen name, test type and time stamp.

4 Experimental Results and Discussions

In this chapter, results from hammer impact test and shaker transducer test will be plotted, compared, and discussed. Important trends will be emphasized.

4.1 Acceleration vs. Force

Motion of specimen after impact is measured in acceleration. In MATLAB file, the data is filtered to avoid noise. Then, to access results, for each impact, the maximum force and accelerations are taken from the original data. They are plotted in following figures. The magnitude of acceleration shows how the motion excited by impact. With same impact force, the lower the acceleration is, the higher the absorbed energy is.

To ease the visual of comparison, data for control specimen is fitted in to curve. The curve type used is 9 order polynomial curve to enhance highest R-square value. It is calculated with following equation, while higher R-square value means the fit curve fitted the data better. The range of it is from 0 to 1. The distribution of measured data and fitted curve is plotted in Figure 11. The R-square value of this fit curve is 0.9530. With this R-square, the fitted curve fit the measured data well. The fitted curve can be used for later comparison between control specimen and hyperdamping specimen.

$\bar{y} = \frac{1}{n}\sum_{i=1}^{n} y_i$, where y indicates data points. [16] ------ (2)

$SS_{tot} = \sum_i (y_i - \bar{y})^2$ [16] ------ (3)

$SS_{res} = \sum_i (y_i - f_i)^2 = \sum_i e_i^2$, where f indicates value calculated by fitted formula [16] ------ (4)

$R^2 = 1 - \frac{SS_{res}}{SS_{tot}}$ [16] ------ (5)

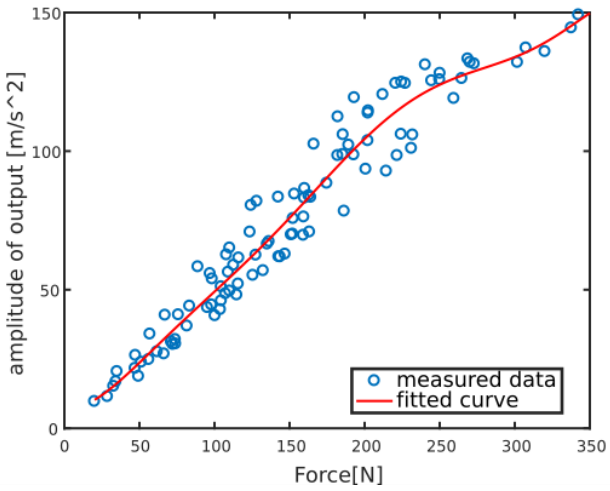

Figure 11: Fitted curve of control specimen

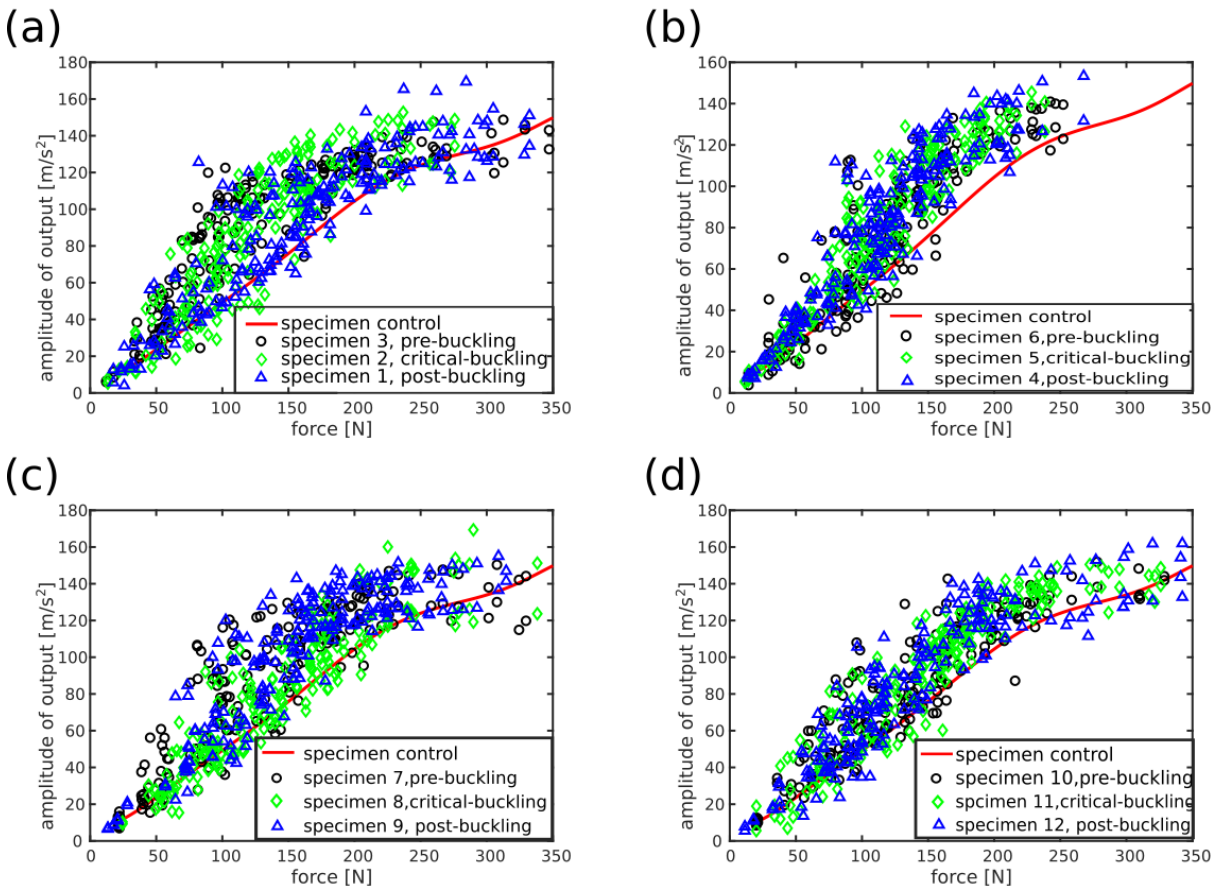

Figure 12: Plot of Accel. vs. Force Plots (a) Comparison of specimens with clear different buckling status. (b) Comparison of specimens with different open angle ratio. (c) Comparison of specimens with different Di/side value. (d) Comparison of specimens with different strain value.

In Figure 12, maximum peak value is shown, with impact force as input and acceleration as output. In Figure 12, the red solid lines represent data measured for control specimen. The black circles show data for pre-buckling specimens (specimen 3, 6, 7, and 10); green diamonds show data for critical-buckling specimens (specimen 2, 5, 8, and 11); and blue triangles show data for post-buckling specimens (specimen 1, 4, 9, 12). Plot (a) aims to study structures at which buckling status can absorb more energy. Plots (b), (c), and (d) are respectively study the roles of open angle ratio, Di/side, and strain.

In Figure 12 (a), the damping effect of hyperdamping material with different buckling status is studied. When force smaller than 150N, most black circles, which are data for pre-buckling specimen, lie above other data sets. When force larger than 150N, most green diamonds, data for critical-buckling specimen, lie above others. Overall, most blue triangles, data for post-buckling specimen, lie below black circles and green diamonds. The red solid line (control specimen) lies at very bottom, but not far from the blue triangles. The trends show post-buckling specimen has lowest acceleration amplitude among all three hyperdamping material specimens, which means more energy is attenuate by it. In addition, none of hyperdamping specimens has lower amplitude than control specimen does. At lower force, blue ones (post-buckling) has

similar value with control specimens, but increase more rapidly when force increase. Thus, control specimen has largest attenuation among four specimens.

In Figure 12 (b), role of open angle ratio is studied. Black circles (specimens with lower open angle ratio), green diamonds (specimens with middle open angle ratio), and blue triangles (specimens with higher open angle ratio) have over all same trend and similar values. At lower force, when smaller than 100N, they distribute along the red solid line. Nevertheless, they have higher value than the red line when force larger than 100N. The comparison shows among these four specimens, when they are excited by force lower than 100 N, hyperdamping specimens absorb similar energy as the control specimen. When specimens are excited by force higher than 100 N, clearly control specimen has lower amplitude. Unfortunately, since difference among three data markers are not clear, role of open angle ratio cannot be concluded.

In Figure 12 (c), role of inner mass diameter, Di/side, is studied. Blue triangles (post-buckling specimens with lower Di/side) and black circles (pre-buckling specimens with lower Di/side) lie above green diamonds (critical-buckling specimens with middle Di/side) in general. The green diamonds lie along the red solid line, and some of them have higher value. Results show middle Di/side, which is 0.22533 (result in 0.00369m inner mass diameter) in this case, can be most efficient to improve the damping performance of hyperdamping material. In addition, this specific parameter combination result in similar attention energy as the control specimen with much lower mass. The sum of mass of control specimen and its metal tube is 18.184g. Moreover, the total mass of this hyperdamping material (green in the plot) and its metal tube is 16.213g. The specimen mass is respectively 6.869g and 8.953g. The difference percent between mass of two specimen is 30%. Similar impact attenuation is achieved with much lower mass.

In Figure 12 (d), role of strain is studied. However, unfortunately, the role is not clear. Trends of three data markers are very close to each other. For all three of them, compare to data for control specimen, similar amplitude is achieved at lower force. And amplitudes become higher that if of control specimen when force are larger than about 100 N.

In previous comparison, specimen 1 and 8 have similar curve with control specimen. To provide a clear comparison, the actual data points of control specimen is plotted with their data points. As shown in Figure 13, for both hyperdamping specimens, control specimen still have lower amplitude. For specimen 1, the amplitudes are overall higher than the control specimen. For specimen 8, at lower force (<100N), the amplitude is similar with it of control specimen with smaller amplitude range. At middle force range (100-250N), the amplitude of hyperdamping specimen is higher that it of control specimen. Then at high force range (>250N), amplitudes become similar again.

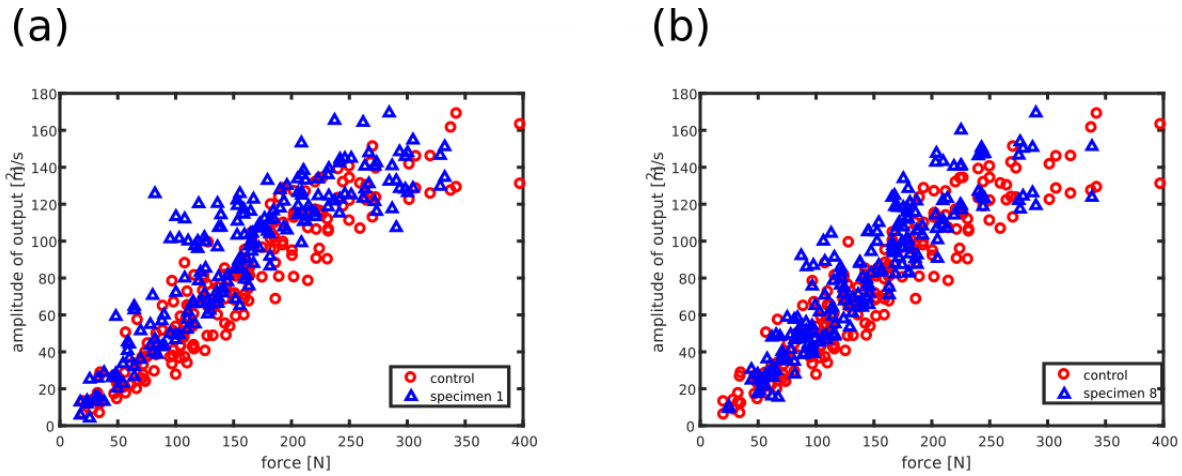

Figure 13: Accel. Data Points Comparison between Control Specimen and (a) specimen 1. (b) specimen 8.

In this term, maximum peak values are compared, indicates specimens' performance at the moment of impact. Lower amplitude is desired. The overall shape of the data points indicates non-linearity. The acceleration increase linearly along with force until about 250N. This phenomenon is identical for all specimens. Combine results from each plot, most hyperdamping specimens have higher amplitude than control specimen does with same impact force applied. The reason might be the larger mass of the control specimen caused it is harder to be excited. Consider the equation of Newton's Second Law, $a = F/m$, with same force applied, larger mass could result in lower acceleration. It is true that excited acceleration of a vibration system is more complicated than Newton's Second Law. But the trend can be analogized. With 20% difference in average in mass, the difference of acceleration is not significant. Some of hyperdamping specimens can even achieve similar energy attenuation as control specimen. Consider the total mass was involved into the structure, hyperdamping material show its achievements in impact energy absorption. Middle Di/side value is preferred, while the roles of open angle ration and strain are not clear. Middle Di/side result in critical-buckling with the specific open angle ration and strain combination in Figure 12 (c). The result matches the hypothesis that critical-buckling structures have better performance in energy absorption.

4.2 Decay Rate vs. Force

The decay rate of impulse response is calculated from exponential fit of amplitude peaks. For each impact, as shown in Figure 14, multiple peaks happen in time response until curve reaches stable. To calculate decay rate, all peaks are fitted in to an exponential curve with equation shows below.

$$Accel = a * e^{b*time} \quad \text{------ (6)}$$

The exponent (value of b) of the fitted exponential equation is defined as decay rate. Unit of it is 1. The higher the magnitude of decay rate is, the more rapid the acceleration decrease with time. Since the decay rates are negative values, lower decay rate indicates more rapid damping effect.

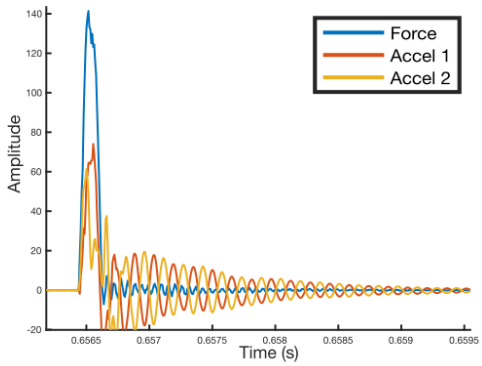

Figure 14: Sample Time Response

The calculated decay rate for each impact is then plotted in response of force. The data sets are grouped in the same way as acceleration results. The red solid lines represent the averaged decay rate for control specimen. The black circles show data for pre-buckling specimens; green diamonds show data for critical-buckling specimens; and blue triangles show data for post-buckling specimens. Plot (a) aims to study structures at which buckling status can absorb more energy. Plots (b), (c), and (d) are respectively study the roles of open angle ratio, Di/side, and strain.

The decay rate data cannot be fitted into a curve with high R-square value. The range and average value of it are interested. However, to provide a comparison throughout the force range, they are fitted into a curve to show the average line. As shown in Figure 15, data points are spread widely about the fitted curve. But the fitted curve approximately show the average throughout the force range. The curve type used in this figure is 4-order polynomial, and the R-square is 0.0682.

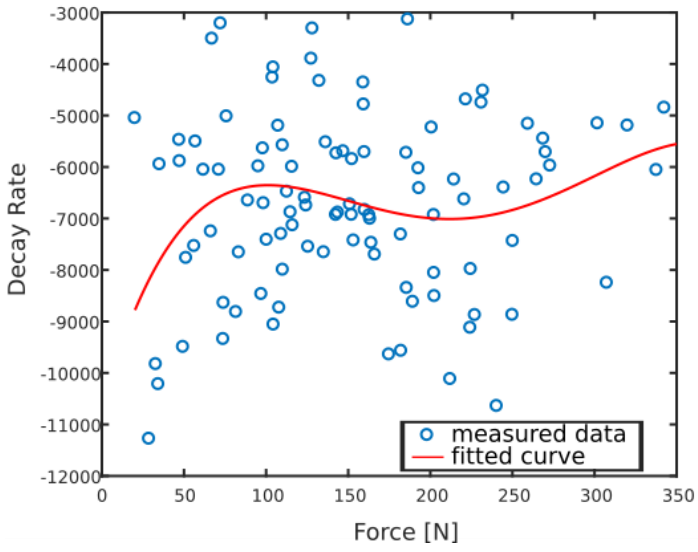

Figure 15: Decay Rate Fit Curve and Data Points

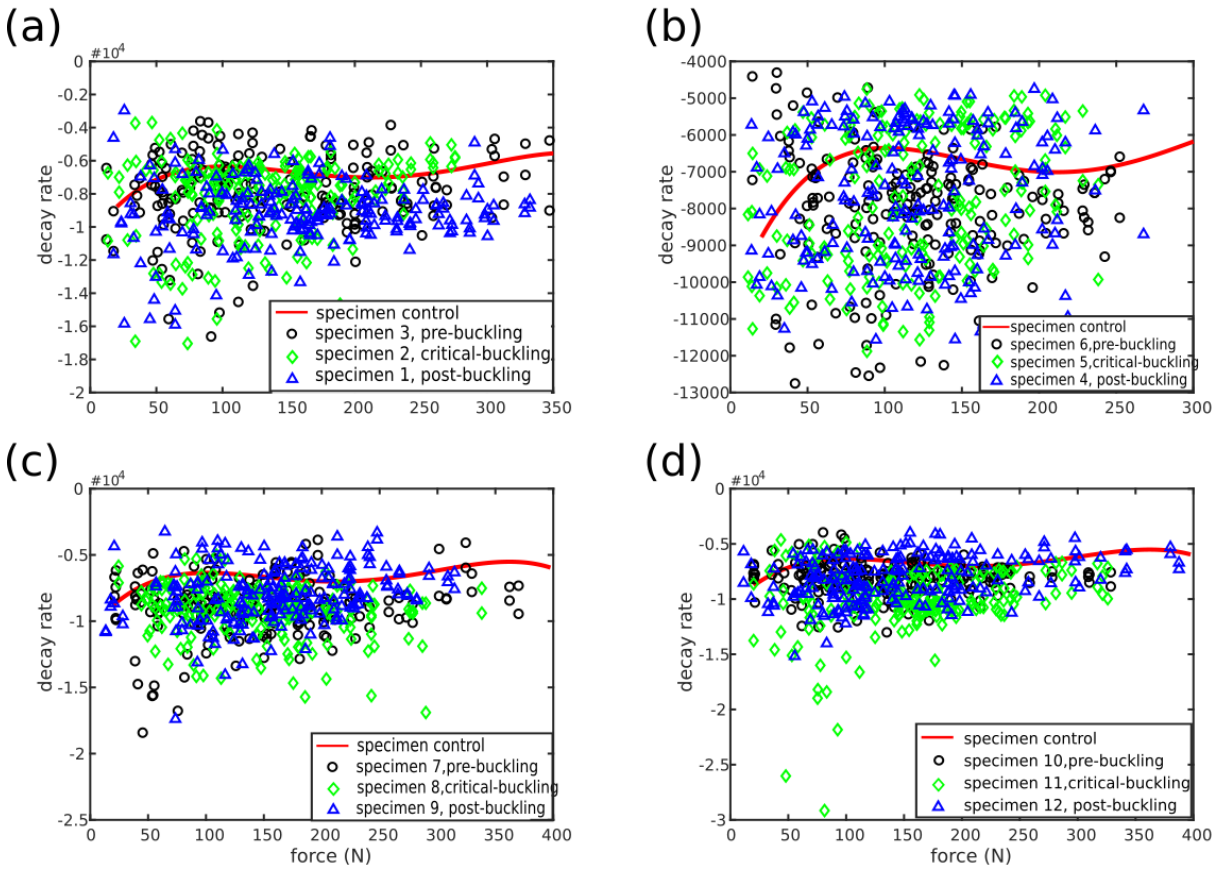

Figure 16: Decay Rate vs. Force (a) Comparison of specimens with clear different buckling status. (b) Comparison of specimens with different open angle ratio. (c) Comparison of specimens with different Di/side value. (d) Comparison of specimens with different strain value.

In Figure 16 (a), three hyperdamping specimens with clear different buckling status are compared with the control specimen. The red solid line, averaged decay rate of control specimen, lies on the upper half plane. Most data markers have lower Y-axis value than it. To compare among three hyperdamping specimens, the blue triangles, which for specimen at post-buckling status, have relative low decay rate among the whole force range. The green diamonds (critical-buckling specimen) and black circles (pre-buckling specimens) have relative high value.

In Figure 16 (b), the role of open angle ratio is studied. Similarly, the red line lies above most of the data makers for hyperdamping specimens. The comparison among three data makers is not achievable from figure. Further comparison will be given with calculated data in Table 8.

In Figure 16 (c), the role of Di/side is studied. Again, the red line for control specimen lies above most of other data points. Relatively, the green diamonds (critical-buckling specimen with middle Di/side) and black circles (pre-buckling specimen with higher Di/side) have lower decay rate. The decay rate of the specimen with lower Di/side is relative high.

In Figure 16 (d), the role of strain is studied. The line of control specimen is in the upper half plain. The trend for hyperdamping specimens are close to each other. Visually, the green diamonds, data for critical-buckling specimen with middle strain, are mostly below the other two.

Table 8: Decay Rate Average and Standard Deviation

specimen #	File Name	Buckling Condition	Decay Rate Mean	Standard Deviation
1	Taper_65625_1_2	Post-Buckling	-9472	342.1
2	Taper_64500_82857_2	Critical-Buckling	-9372	2080
3	Taper_63750_72143_2	Pre-Buckling	-5202	85.97
4	Taper_64531_1_22588	Post-Buckling	-11180	4300
5	Taper_64531_87143_22588	Critical-Buckling	-9676	2252
6	Taper_64531_7_22588	Pre-Buckling	-8246	1428
7	Taper_64500_1_3	Pre-Buckling	-8330	2283
8	Taper_64500_1_22533	Critical-Buckling	-6660	1144
9	Taper_64500_1_16	Post-Buckling	-8033	896.9
10	Taper_63750_7_20667	Pre-Buckling	-8157	99.91
11	Taper_64750_7_20667	Critical-Buckling	-9739	2.738
12	Taper_65500_7_20667	Post-Buckling	-10148	326.5
20	Control	N/A	-6720	2521

To provide a clear comparison, Table 8 shows the overall average for decay rate of each specimen. Label colors in the table match the data curves and data points in the figures. Blue represent post-buckling specimens; green represents critical-buckling specimens; black represents pre-buckling specimens. The control specimen has average decay rate of -6720, which is the third highest value in the table. Thus, it can be concluded that almost all specimens can provide faster decay to the acceleration, which means they can absorb more energy during oscillation relative to control specimen.

The comparison of specimen 1, 2, and 3 is a comparison among specimens with clear different buckling status. Specimen 1 and 2, respectively at post-buckling and critical-buckling, have negative nine-thousands decay rate, while the specimen 3 have a higher value. From the comparison, hyperdamping material that buckled tends to attenuate impact more rapidly.

Comparison of specimen 4, 5, and 6 studies the role of open angle ratio. Specimen 4, the one at post-buckling with highest open angle ratio, has the lowest decay rate. Specimen 6, the one at pre-buckling with

lowest open angle ratio, has the highest decay rate. Thus, specimens with higher open angle ratio would absorb energy more rapidly.

To study the role of Di/side, specimens 7, 8, and 9 can be compared. Specimen 7 and 9, which are respectively at pre-buckling and post-buckling have lower decay rate than it of specimen 8. Thus, specimen with middle Di/side value tends to attenuate the amplitude slower than others. Recall in Chapter 4.1, middle Di/side value causes the lowest amplitude with same exciting force. Therefore, the inefficiency in decay rate of middle Di/side might result in that a lot energy, namely, amplitude, has already been attenuated at the first peak, when the specimen is just excited.

Specimen 10, 11, and 12 studies the role of strain. The rank of decay rate from high to low is decay rates of specimen 10, 11, and 12. They are respectively specimens with strain from low to high. Thus, specimens with higher strain applied can absorb more energy.

Specimen 8 has similar average decay rate as control specimen, while specimen 3 has higher decay rate. Data points from these two specimens are plotted with control specimen to provide more accurate comparison. From Figure 17, specimen 3 has similar distribution with control specimen. And specimen 8 has lower decay rate than the control specimen. The reason of the difference between average comparison and data points comparison might be the broader range of the control specimen. It can result in error in average calculation.

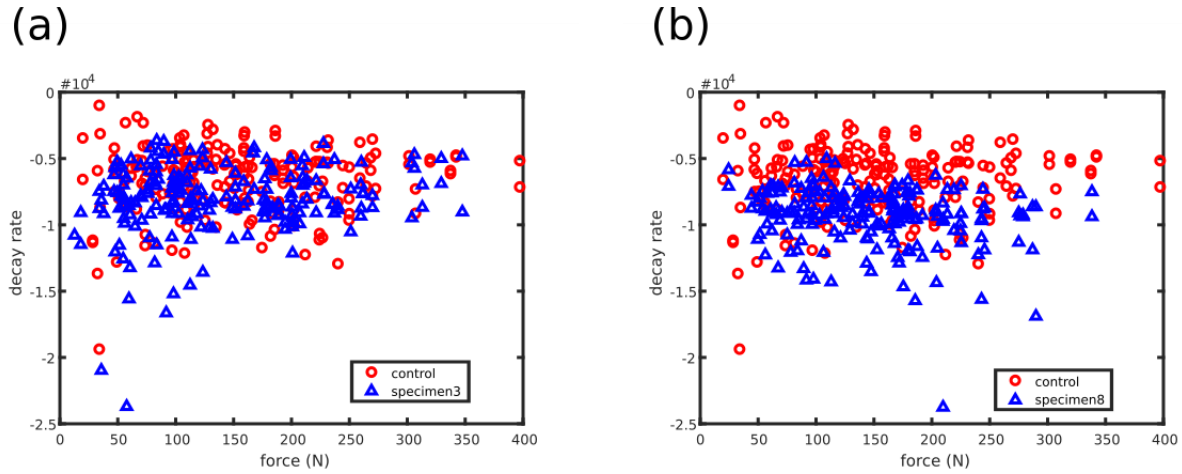

Figure 17: Decay Rate Data Point Comparison between Control Specimen and (a) Specimen 3. (b) Specimen 8.

From the Table 8, specimen 11 and specimen 12 have extremely low decay rate with low standard deviation. To provide a visual comparison, it is plotted with control specimen. In Figure 18 (a), hyperdamping specimen has clearly lower decay rate than the control specimen. In figure (b), decay rate for both specimens are similar at high force range (>250 N). At lower force range (<250N), the decay rate range of hyperdamping specimen is from -13,000 to -5,000, while it is from -13,000 to -2,000 for control specimen. With similar lower range, lower upper range decides that hyperdamping specimen has lower average decay rate.

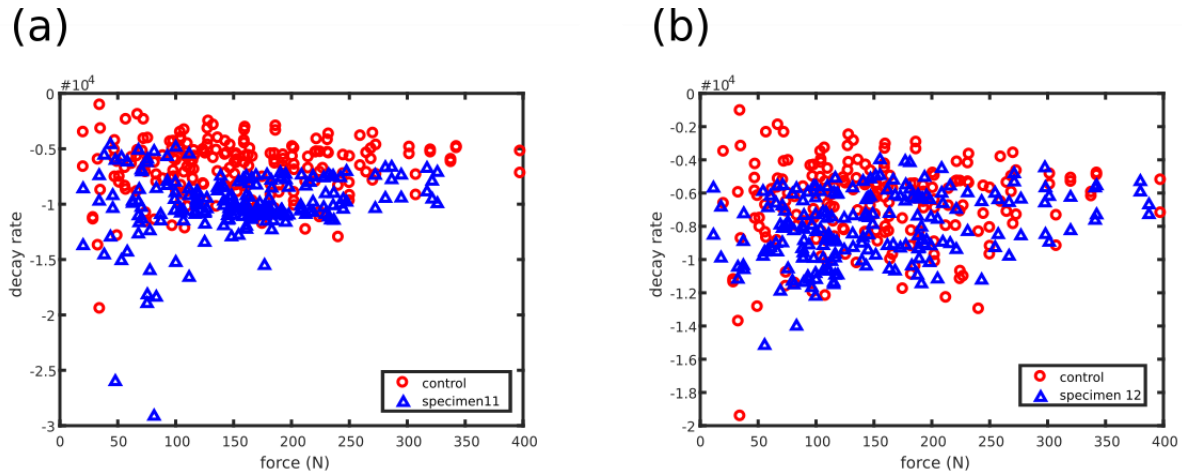

Figure 18: Decay Rate Data Points Comparison between Control Specimen and (a) specimen 11. (b) specimen 12.

Overall, all hyperdamping specimens show better performance than the control specimen in decay rate. With big mass can help it to obtain a lower excited acceleration, control specimen cannot attenuate the existing acceleration rapidly. Once the specimen is excited, beams in the geometry start to show their effects as discussed in Chapter 1. In conclusion, specimens are post-buckling with higher open angle ratio and higher strain applied tend to show better performance in decay rate analysis. Apply the conclusion to beams in the geometry, more slender and more bucked beams have better performance. This result is different from the hypothesis that critical-buckling beams are supposed to have better performance. The difference might come from the fabrication error. Refer Table 7, the highest measured error of strain is 16% for the tapered design, while the error in open angle ratio and Di/Side is unable to be measured. Therefore, the buckling status might be different from designed. During experiment, visually, specimen 12 has already been observed as not-buckling, while it is designed as post-buckling. And critical-buckling specimens cannot be determined visually if they are in correct status. Slight difference in parameters can result in change of buckling status. The buckling status is also affected by material properties. Even though the material properties are determined experimentally before testing, it is still possible that they are different among each time fabrication. With a higher decay rate, they could attenuate the impact energy more rapidly. In general, Hyperdamping material has better performance in this term than the control specimen does. With hyperdamping material, the impact energy applied on the structure can be absorbed fast.

4.3 Average Decay Rate vs. Mass

In the Figure 19, the decay rate is plotted in terms of mass of specimen. Here, the mass is the sum of the specimen itself and the metal tube contains it. The reason that the total mass is used is that different metal tubes are used for different specimens. The mass of the tube would also affect the experiment results.

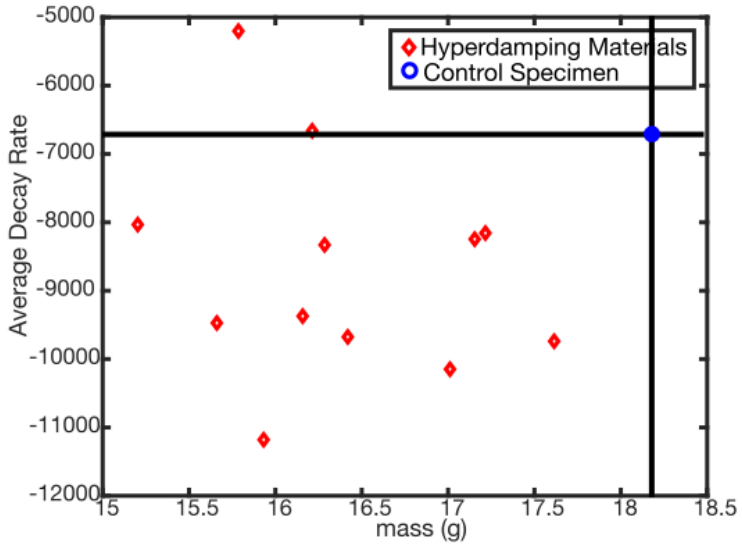

Figure 19: Average Decay Rate vs. Mass, comparison between hyperdamping material and control specimen

In Figure 19, blue circle is data for control specimen, and red diamonds are data for hyperdamping materials. Ten out twelve red diamonds have lower value in both x and y axis compare to the blue circle. The trend shows most hyperdamping specimens can attenuate impact energy more rapidly with lighter mass introduce to the structure system.

4.4 One-third Octave Bands

The concept of octave bands is introduced to simplify study in frequency range. A frequency range called octave band when the highest frequency is twice of the lowest frequency. A one-third octave band is defined as a frequency band whose highest frequency f_2 is the lowest frequency f_1 times the cube root of two.

$$f_2 = f_1 \times \sqrt[3]{2} \quad \text{------ (7)}$$

Mathematically, the one third octave band is defined as following.

The frequency range is divided into 31 one-third bands. The center of each band is defined as equation (8). The parameter "a" is an integer vector from -18 to 14.

$$f_{center} = 10^3 \times 2^{a/3} \quad \text{------ (8)}$$

$$f_d = 2^{1/6} \quad \text{------ (9)}$$

$$f_{high} = f_{center} \times f_d \quad \text{------ (10)}$$

$$f_{low} = f_{center} / f_d \quad \text{------ (11)}$$

The amplitude in each octave band is calculated as the square root of the sum of square of amplitudes from lowest frequency highest frequency. The value is then transferred into dB. The mathematical equation can be represented as follow.

$$A = 10 \log_{10}\left(\sqrt{\sum_{f_{low} \to f_{high}} Amplitude^2}\right) \quad \text{------ (12)}$$

4.5 Hammer Impact Testing 1/3 Octave Band Results

With mathematics showing in 4.4, the acceleration amplitude is averaged among an octave band. The amplitudes is then plot in frequency range.

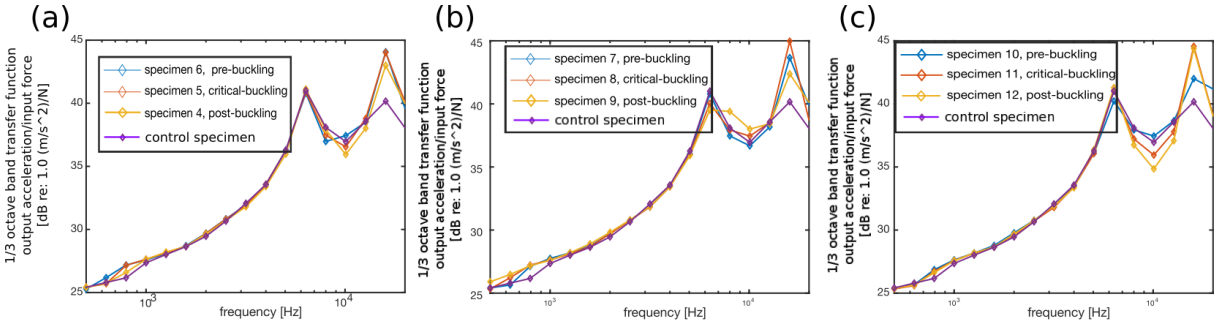

Figure 20: 1/3 band transmissibility over frequency plot of tapered design with (a) strain (b) Di/side (c) open angle ratio as interested parameter. Comparisons are made among curves with colors of purple, control specimen, yellow, post-buckling specimen, blue, pre-buckling specimen, and red, critical-buckling specimen.

Figure 20 shows the trends of 1/3 octave band transmissibility of the tapered design. Here, the transmissibility is defined as the ratio of the frequency responses of acceleration to force. Figure 20 (a) compares results of specimens with different value of strain, while Di/side and open angle ratio are constant. Figure 20 (b) compares results of specimens with different value of Di/side. Figure 20 (c) compares results of specimens with different value of open angle ratio. The purple curve and data points in all figures are the data generated from the control specimen made on solid elastomer. In all figures, data of control specimen is lower than the others, which means no hyperdamping specimen has larger damping than control specimen. This might result from the damping caused by the large mass of control specimen.

From 1000 Hz to about 10000 Hz, in all plots, data curves are close to each other. A drop happened at about 10000 Hz. At this drop, in figure (a) and (c), the yellow curve, which shows post-buckling specimens has the lowest value. In figure (b), blue curve, which show data for pre-buckling specimen, has the lowest value. It suggests that lower Di/side, higher strain and higher open angle ratio improve specimens' performance at 10000 Hz vibration.

Then, a peak happens after 10000 Hz. In all three plots in Figure 20, the purple curve with data for control specimen has the lowest value. It states that control has better attenuation performance for vibrations within higher than 10000 Hz frequency.

The unclear trend in Figure 20 suggests that, no matter hyperdamping material or control specimen, their damping effects do not vary significantly along frequency.

4.6 Shaker Testing Results for Tapered Design

For shaker transducer test, the frequency response is interested. To present results, the concept of transmissibility is defined. It is ratio between input and output. In the test, the input is measured as force, while the output is measured as acceleration. Thus,

$$transmissibility = \frac{acceleration}{force}[(m/s^2)/N] \quad \text{------ (13)}$$

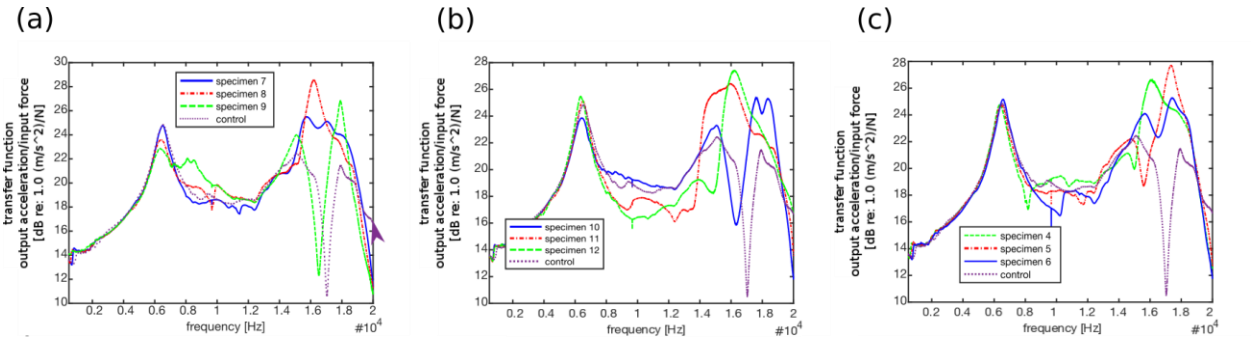

Figure 21: Transmissibility amplitude among certain range of frequency for specimens with (a) Di/side value (b) strain, and (c) open angle ratio as interested parameters. Here, green dotted curves show results of post-buckling structure, red dotted curves show results of critical-buckling structure, blue solid curves show results of pre-buckling structure, and purple curves show results of control specimen.

In the transfer function plot (Figure 21), the mainly interested frequency range is from 8000Hz to 14,000Hz, frequency range between two peaks, where the dynamic behaviors are distinct among specimens.

In Figure 21 (a), role of Di/side value is studied. Smaller Di/side value result in buckle of structure. In the interested range, the specimen 9 lies close to specimen 8 curve, on top of specimen 7 and control specimen curve. The specimen 7 curve, which represents pre-buckling structure, has the smallest value of transmissibility. As stated before, transmissibility is calculated as a ratio between output amplitude and input force. The lower the transmissibility is, the lower the acceleration is with same force applied. Thus, it can be concluded that larger Di/side value enhances the absorption of wave energy, which is close to the performance of control specimen.

In Figure 21 (b), curves differ from each other clearly. Role of strain is studied in comparison within this plot. Larger strain value result in buckle of structure. In the interested range, control specimen curve lies above the specimen 11 curve and below the specimen 10 one. The specimen 12 curve, which represents post-buckling structures, has the overall smallest value of transmissibility in the interesting range. Thus, larger strain enhances the absorption of wave energy.

In Figure 21 (c), role of open angle ratio is studied. Larger open angle ratio result in buckle of structure. In the interested range, the control specimen curve lies between specimen 4 curve on top and specimen 5 one

on bottom. The specimen 6 curve, which represents pre-buckling structure, has the smallest value of transmissibility. Thus, smaller open angle ratio enhances the absorption of wave energy.

Combine the results from three plots, most of specimens with topology design have lower value of transmissibility at the interested frequency range than the controlled specimen does, which does not have geometry design. Thus, the tapered design shows good performance in absorption of wave energy. To sum the role of parameter, according to comparison, specimens with larger strain, larger Di/side and smaller open angle ratio. Trends of these parameters guide to different buckling status. Thus, the role of buckling status is not comparable.

4.7 Shaker Results with Periodic Voids Design

In Figure 22 (a), role of voids number is studied. As porosity and strain identical, n=5, result in buckle of structure. In the interested range from 6,000 Hz to 14,000 Hz, the specimen 13 curve lies at very bottom and away from other data curves. It shows that the specimen with n=3 and pre-buckling status tends to have much better attenuation performance at the interesting frequency range. Compared among the other three, control specimen curve has the second lowest at this range, and specimen 18 curve and specimen 19 curve have similar results. Thus, fewer voids number enhances the absorption of wave energy with other parameters the same. Other two hyperdamping specimens have slighter attenuation compare to the control specimen.

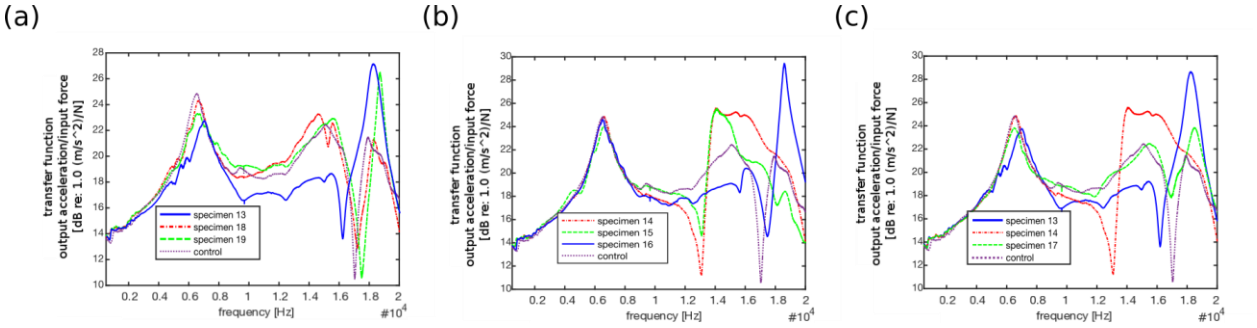

Figure 22: Transmissibility amplitude among certain range of frequency for specimens with (a) voids number, (b) porosity, and (c) strain. Here, green dotted curves show results of post-buckling structure, red dotted curves show results of critical-buckling structure, blue solid curves show results of pre-buckling structure, and purple curves show results of control specimen.

In Figure 22 (b), role of porosity is studied. Larger porosity value result in buckle of structure. Between 6,000Hz to 16,000Hz, control specimen curve is higher than the specimen 16 curve. Lower transmissibility means better vibration control performance. Thus, hyperdamping specimens enhance the absorption of wave energy. Specimen 14 and 15 have a big jump at about 13,000 Hz. They respectively have similar value with specimen 16 and control specimen at frequency lower than 12,000 Hz. After the drop at 13,000 Hz, they jumps to highest transmissibility. The jump shows these two specific specimens have a relative narrow band operation frequency range compare to others. Comparison within 6,000 Hz to 12,000 Hz shows lower porosity have better attenuation performance.

In Figure 22 (c), the role of strain is studied. Larger strain result in buckle of structure. Same with last plot, specimen 14 undergoes a big drop and jump at about 13,000 Hz, from the second lowest to the lowest and then to the highest. In the frequency range of 6,000 Hz to 16,000 Hz, specimen 13 curve lies at very bottom. The specimen 17 curve and control specimen curve are at top. The specimen 13 curve, which represents pre-buckling structure, has the smallest value of transmissibility. Thus, smaller strain enhances the absorption of wave energy.

In all three figures, pre-buckled structures show best performance of wave energy absorption. Periodic voids designs with less voids number, smaller porosity and smaller strain can absorb more wave energy when excited.

Combine the results from three plots, most of specimens with topology design have lower value of transmissibility at the interested frequency range than the controlled specimen does, which does not have geometry design. However, two out of seven specimens show narrowband damping effect. Thus, the periodic voids design shows good performance in absorption of wave energy with some parameter combinations work with relative narrowband frequency.

4.8 Role of Mass in the Damping Effect

According to the frequency range of result data, two frequency ranges are selected to average the transmissibility amplitudes.

$$A = 10\log_{10}\left(\sqrt{\sum_{f_{low}\to f_{high}} Amplitude^2}\right) \qquad \text{------ (14)}$$

Here we consider $f_{low} = 2{,}000Hz$ and $f_{high} = 10{,}000Hz$.

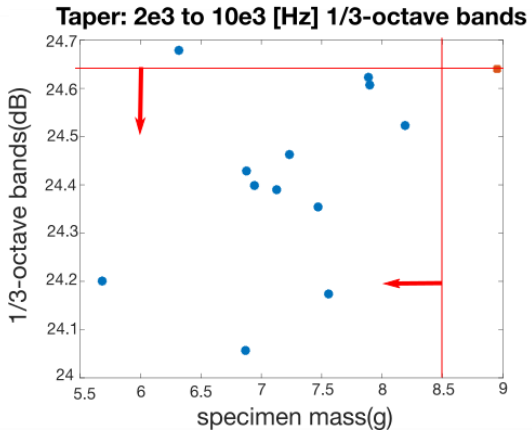

Figure 23: Distribution of 1/3 octave band transmissibility over mass for tapered design, where the transmissibility is averaged over frequency range of (a) [2000, 10000] Hz (b) [12500, 20000] Hz. Here, red data point represents result for the controlled specimen, and blue da points represent result for tapered design specimens.

The damping effects have been observed in above experimental results. However, common sense implies mass of material is also a significant source of damping. Larger mass required higher energy to excite. [17]

To study the role mass in energy absorption in the designs, the averaged transmissibility over certain range is plotted in terms of specimen mass.

For the tapered design, as shown in Figure 23, in the frequency range of [2000, 10000] Hz, data points for specimens with topology design are distributed at the lower left corner, while the data point for controlled specimen is at upper right corner. Thus, in this frequency range, the tapered design specimens generate larger damping with lower mass satisfied the requirement of lightweight material system. The average of 12 specimens is 24.4dB, while the amplitude for control specimen is 24.6dB. The amplitude decreased by 0.2 dB.

For some extreme cases, the lowest mass is 5.682g (36.5% lower), with a 24.20 dB amplitude (0.4 dB lower). The lowest amplitude is 24.06 dB (0.54 dB lower), with a 6.869g mass (23.3 lower).

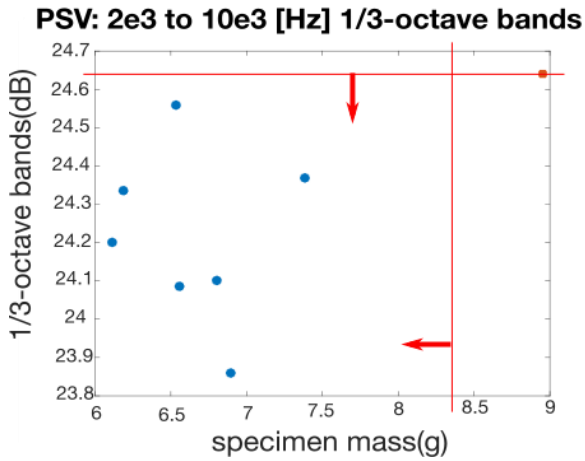

Figure 24: Distribution of 1/3 octave band transmissibility over mass for periodic voids design, where the transmissibility is averaged over frequency range of (a) [2000, 10000] Hz (b) [12500, 20000] Hz. Here, red data point represents result for the controlled specimen, and blue da points represent result for periodic voids specimens.

The result for periodic void design is similar as it for tapered design, shown in Figure 24. In low frequency range, the periodic voids design specimens generate larger damping with lower mass satisfied the requirement of lightweight material system. In the high frequency range, the periodic voids design specimens do not generate damping as high as the controlled specimen does. Yet, they involve lighter mass to the system. The average mass of periodic voids design is 6.639g, 26% lower than the control specimen. The average of seven hyperdamping specimen is 24.2 dB, while it is 24.6 dB for control specimen. It is decreased by 0.4 dB.

For extreme cases, lowest mass in this design is 6.113 g (31.7% lower), with 24.20 dB (0.4 dB lower). The lowest amplitude is 23.86 dB (0.74 dB lower).

5 Conclusions

After discussing the results from both testing, both designs show capability of energy absorption for vibration, wave energy.

The hammer impact testing shows tapered design can absorb energy immediately after the impact, and can provide a rapid drop in amplitude after the first peak. The comparison of acceleration right after the impact shows that hyperdamping specimens undergo slightly greater instantaneous acceleration after the impact compare to the control specimen. Two of specimens even have very similar range and trends as the control specimen does, especially when impact force lower than 250N. Consider the role of mass, the average of mass of tapered design specimen is 7.171g, while it is 8.953g for control specimen. With tapered design, mass is reduced 20% with similar damping effects for impact. Tapered design shows even better performance in decay rate, which represent how rapid the amplitude drops after the impact. Ten out of twelve hyperdamping specimens have lower decay rate than the control specimen, which means more rapid drop. The other two, even though have higher average decay rate, their data points show lower decay rate in figures. Overall, all hyperdamping specimens have better decay rate than the control specimen. The one-third octave band frequency response shows damping effects of hyperdamping specimens do not vary along frequencies for vibration caused by impact.

The shaker transducer test show performance of both hyperdamping designs in wave energy absorption. The tapered design have broadband damping effects. Topologies with larger strain, larger Di/side and smaller open angle ratio have better energy attenuation, while the role of buckling status is not achievable with this result. Consider the role of mass, with 20% mass decrease, averaged amplitudes of 11 out of 12 hyperdamping specimens are lower than it of control specimen at frequency range from 2,000Hz to 10,000Hz.

For the periodic voids design, 2 out of 7 specimens show relative narrow band effects. The “narrowband” is 6,000 Hz to 12,000 Hz, which is already a very broad frequency range. Pre-buckled structures show best performance of wave energy absorption. Periodic voids designs with less voids number, smaller porosity and smaller strain can absorb more wave energy when excited. Periodic voids design can result in lower average amplitudes among frequency range 2,000Hz to 10,000Hz.

Overall, for absorption of wave energy, periodic voids design shows better performance in decreasing mass, while tapered design shows better broad band effects.

Throughout the research, the role of buckling status does not perform in a constant trend. It might result from the fabrication error. Measured strain shows slight error while other parameters, such as the angle of tapering, are not measurable using the current methods. As a result, specimens might not in the buckling status as ideally intended. One conclusion from this result is that the hyperdamping phenomena leveraged here are robust to parameter deviation from ideal values.

5.1 Recommendations for Future Work

This research concludes initial success in square-shaped cross-section hyperdamping design. For future study, more specimens with different mass should be fabricated and tested to fill the curve of how averaging transmissibility in low and high frequency range acts to mass. A new impact testing setup should be designed to allow testing for both design, and to minimize the effects caused by other material in the testing setup system. In addition, a more refined fabrication method is desirable to be found to provide the specimens with more accurate parameters.

BIBLIOGRAPHY

[1] Benaroya, H; Nagurka , M L, *Mechanical Vibration: Analysis Uncertainties, and Control, Third Edition*.: CRC Press, 2009.

[2] Shim, J; Shan, S.; Kosmrlj, A.; Kang, S. H.; Chen, E. R.; Weaver, J. C.; Bertoldi, K., "Harnessing Instabilities for Design of Soft Reconfigurable Auxetic/Chiral Materials," *Soft Matter*, pp. 8198-8202, Sep. 2013.

[3] Wang, P.; Casadei, F.; Shan, S.; Weaver, J. C.; Bertoldi, K., "Harness Buckling to Design Tunable Locally Resonant Acoustic Metamaterials," *Physical Review Letters*, July 2014.

[4] Nouh, M.; Aldraihem, O.; and Baz, A., "Wave Propagation in Metamaterial Plates with Periodic Local Resonances," *Journal of Sound and Vibration*, pp. 53-73.

[5] Baravelli, E; Ruzzene, M, "Internally Resonating Lattices for Bandgap Generation and Low-frequency Vibration Control," *Journal of Sound and Vibration*, pp. 6562-6579, 2013.

[6] Florijin, B; Coulais, C; Hecke, M V, "Programmable Mechanical Metamaterials," *Physical Review Letters*, Oct. 2014.

[7] Rafsanjani, A.; Akbarzadeh, A.; Pasini, D., "Snapping Mechanical Metamaterials under Tension," *Advanced Materials*, 2015.

[8] Harne, Ryan L.; Song, Yu; Dai, Quanqi, "Trapping and attenuating broadband vibroacoustic energy with hyperdamping metamaterials," *Extreme Mechanics Letters*, May 2016.

[9] Bishop, Justin; Dai, Quanqi; Song, Yu; Harne, Ryan L., "Resilience to Impact by Extreme Energy Absorption in Lightweight Material Inclusions Constrained Near a Critical Point," *Advanced Engineering Materials*, 2016.

[10] Brodt, M.; Lakes, R. S., "Composite Materials Which Exhibit High Stiffness and High Viscoelastic Damping," *Journal of Composite Materials*, Sep. 1995.

[11] Hu, Nan,; Burgueño, Rigoberto, "Buckling-induced smart applications: recent advances and trends," *Smart Materials and Structures*, 2015.

[12] Kochmann Dennis M., "Stable extreme damping in viscoelastic two-phase composites withnon-positive-definite phases close to the loss of stability," *Mechanics Research Communications*, pp. 36-45, Sep. 2013.

[13] Antoniadis, I.; D, Chronopoulos; V, Spitas; D, Koulocheris, "Hyper-dampingpropertiesofastiffandstablelinearoscillator with anegativestiffnesselement," *JournalofSoundandVibration*, pp. 37-52, 2015.

[14] Gürgözea, M.; Doğruoğlub, A.N.; Zerena, S., "On the eigencharacteristics of a cantilevered visco-elastic beam carrying a tip mass and its representation by a spring-damper-mass system," *Journal of Sound and Vibration*, pp. 420-426, Mar. 2007.

[15] Daryl L. Logan, *A first course in the finite element method*.: Thomson, 2011.

[16] Damodar N. Gujarati, *Basic Econometics*. New York: McGraw-Hill Companies, 2009.

[17] William J. Palm, *System Dynamics*.: Mc-Graw Hill Companies, 2010.

6 Appendix

6.1 Sample MATLAB Code

6.1.1 MATLAB code for FEM result data analysis

```
clear all
clc
fid='Di_7_strain_02_12_17_PrestressedEigenfrequency_TaperOutIn.txt';
data=dlmread(fid);
tube_side_length=0.625;
%% grab from the data output
v.dh=data(:,1); % grab first index, which are the values of the parameter
(either outer/inner/all solutions from matlab)
v.eigenfreq=data(:,2); % grab second index column which are the
eigenfrequencies [Hz]
%% parameters Taper
v.b_a=0.7;%linspace(0.7,1,15);%Open Angle Ratio
v.D_side=linspace(0.16,0.3,16);%inner diameter/side_length
v.side=linspace(1.02,1.05,16);%side_length=strain*tube_side_length
v.num_eig_freqs=50; % number of eigenfrequencies recorded
v.eigs=reshape(v.eigenfreq,[length(v.side),length(v.D_side),v.num_eig_freqs])
;
% v.eigs=reshape(v.eigenfreq,[v.num_eig_freqs,length(v.side),length(v.b_a)]);
%
v.eigs=reshape(v.eigenfreq,[v.num_eig_freqs,length(v.side),length(v.D_side)])
;
%% plot taper
% close all
axis1=['b/a, open angle ratio'];
axis2=['D/side, inner mass diameter/side length'];
axis3=['strain percent'];
% for iii=1:length(v.b_a)
%     figure(iii);
%     clf;
%     plot(v.side,squeeze(v.eigs(iii,:,:)),'-');
%     xlabel(axis3);
%     ylabel('eigenfrequency [Hz]');
%     titlename2=['b/a, open angle ratio =' num2str(v.b_a(iii),'%1.4f'),'
D/side=0.2' ];
% %     titlename3=['Strain =' num2str(v.side(iii),'%1.4f'),'in','
D/side=0.2'  ];
%     title({titlename2});
% end
% for iii=1:length(v.D_side)
%     figure(iii);
%     clf;
%     plot(v.b_a,squeeze(v.eigs(:,iii,:)),'-');
%     xlabel(axis1);
%     ylabel('eigenfrequency [Hz]');
%     titlename1=['D/side, inner mass diameter/side length
=',num2str(v.D_side(iii),'%1.4f'),' strain=3.25%' ];
%     title({titlename1});
% end
% for iii=1:length(v.side)
%     figure(iii);
%     clf;
```

```
%     plot(v.b_a,squeeze(v.eigs(iii,:,:)),'-');
%     xlabel(axis1);
%     ylabel('eigenfrequency [Hz]');
%     titlename3=['strain =' num2str(v.side(iii),'%1.4f'),'Di/side=0.2'];
%     title({titlename3});
% end
%% contour
    figure(1);
    clf;
    contourf(v.side,v.D_side,squeeze(v.eigs(:,:,1))',20,'linestyle','none');
    xlabel(axis3);
    ylabel(axis2);
    titlename4=['Eigenfrequency [Hz] Fundamental B/A=0.7'];
    title({titlename4})
    colorbar
%% parameter periodic
% v.out_layer=0.78;
% v.porosity=linspace(0.45,0.65,15)*v.out_layer^2;
% v.n=3:5;
% v.strain=1.07;%linspace(1.04,1.07,15);
% v.num_eig_freqs=50; % number of eigenfrequencies recorded
%
v.eigs=reshape(v.eigenfreq,[length(v.n),length(v.porosity),v.num_eig_freqs]);
% axis4=['pososity, voids area/total area'];
% axis5=['strain percent, side length/tube side length'];
% axis6=['voids number'];
% % plot periodic
% close all
% for iii=1:length(v.n)
%
%     plot(v.porosity,squeeze(v.eigs(iii,:,1)),'-');
%     hold on
% end
% for iii=1:length(v.strain)
%     figure(iii);
%     clf;
%     plot(v.porosity,squeeze(v.eigs(iii,:,:)),'-');
%     xlabel(axis4);
%     ylabel('eigenfrequency [Hz]');
% %     titlename4=['porosity =' num2str(v.porosity(iii),'%1.4f'),' n=3' ];
%     titlename3=['Strain =' num2str(v.strain(iii),'%1.4f'),'in',' n=3'  ];
%     title({titlename3});
% end
% for iii=1:length(v.n)
%     figure(iii);
%     clf;
%     plot(v.porosity,squeeze(v.eigs(iii,:,:)),'-');
%     xlabel(axis4);
%     ylabel('eigenfrequency [Hz]');
% %     titlename4=['porosity =' num2str(v.porosity(iii),'%1.4f'),' n=3' ];
%     titlename3=['n =' num2str(v.n(iii),'%1.0f'),'in',' strain=7%'  ];
%     title({titlename3});
% end
% for iii=1:length(v.porosity)
%     figure(iii);
%     clf;
%     plot(v.n,squeeze(v.eigs(:,iii,:)),'-');
```

```
%     xlabel(axis4);
%     ylabel('eigenfrequency [Hz]');
%     titlename4=['porosity =' num2str(v.porosity(iii),'%1.4f'),' strain=7%'
];
% %     titlename3=['Strain =' num2str(v.side(iii),'%1.4f'),'in','
D/side=0.2'  ];
%     title({titlename4});
% end
%     xlabel(axis4);
%     ylabel('eigenfrequency [Hz]');
%     titlename2=['n, voids number =' num2str(v.n(iii),'%1.2f') ];
% %     titlename3=['sideLength =' num2str(v.side(iii),'%1.2f'),'in' ];
%     title('Eigenfrequency at Strain=5%');
%     legend('n=3','n=4','n=5')
% end
% hold off
% % Contour
% figure(iii+1);
%     clf;
%     contourf(v.n,v.porosity,squeeze(v.eigs(:,:,1))',20,'linestyle','none');
%     ylabel(axis4);
%     xlabel(axis6);
%     titlename4=['Eigenfrequency [Hz] Fundamental Solution strain=5%'];
%     title({titlename4})
%     colorbar
```

6.1.2 Data acquisition for Hammer Impact Test

```
%% data acquisition toolbox NI
clear all
warning off

%% plot styles
colors=['k' 'r' 'g' 'b' 'm' 'k' 'r' 'g' 'b' 'c' 'm'];
mtypes=['o' 'v' 's' '^' 'd' 'o' 'v' 's' '^' 'x' 'd'];

%% acquire data?
dataacquire=1; % yes for acquire

%% data acquisition setup parameters
d.fs=65536*2; % sampling frequency [Hz]. Chosen so that each impact peak has
~4 data points to avoid aliasing
d.seconds=2; % [s] seconds of data acquisition

d.filter_data_lo=50; % [Hz] low-pass digital filter frequency
d.filter_data_hi=18000; % [Hz] high-pass digital filter frequency

%% filter create
%
myfilt=designfilt('lowpassiir','filterorder',2,'passbandfrequency',d.filter_d
ata_hi,'PassbandRipple',0.01,'samplerate',d.fs);
myfilt=designfilt('bandpassiir','filterorder',2,'HalfPowerFrequency1',d.filte
r_data_lo,'HalfPowerFrequency2',d.filter_data_hi,'samplerate',d.fs); % filter
result

%% parameters for hammer impact
d.numoutputs=2; % number of simultaneous output sensor locations
d.numlocs=1; % number of input locations on beam
d.numhits=100; % target number of(modal hammer impacts) per location
d.threshold_impact_force=10; % [N] any force above this level is flagged as
an impact event
d.time_fft=.05; % [s] time to collect data after each impact
d.sec_jump=.01; % TUNABLE PARAMETER [s] seconds to jump forward after each
impact registration. Each impact must occur in less time than this value

%% test specimen name, parameters, filenumber if need more than 1
d.specimen='Control'; % specimen name, or no_specimen if none

%% filename for save d structure
c=clock;
d.filename=[num2str(c(1)) '_' num2str(c(2),'%02.0f') '_'
num2str(c(3),'%02.0f') '_' num2str(c(4),'%02.0f') '_' num2str(c(5),'%02.0f')
'_' num2str(c(6),'%02.0f') '_hammer_' d.specimen '_impact.mat'];
saveon=1; %overwrite is not possible due to timestamp in filename

%% sensor sensitivity
d.sensor{1}='PCB_086C01_SN37316_force_transducer_impact_hammer';
d.ch_sens(1)=1/0.01108; % N/V
d.sensor{2}='PCB_U352A10_SN4617_mini_accelerometer';
d.ch_sens(2)=14.06442964; % (m/s^2)/V
d.sensor{3}='PCB_U352A10_SN4618_mini_accelerometer';
```

```
d.ch_sens(3)=16.9600475; % (m/s^2)/V

d.nn_chan=length(d.ch_sens);

%% mean sensor values, this only plays a role in determining mean-square
responses if relevant
d.data_mean(1)=0; % mean force transducer voltage [V]
for iii=1:d.numoutputs
    d.data_mean(iii+1)=0; % mean accel sensor voltage [V]
end

%% if for data acquisition
if dataacquire==1 % 1=yes for acquire
    %% identify connected devices
    devices=daq.getDevices;
    %once obtained, ensure using correct device name in below session and
acquire lines

%% data acquisition setup
s=daq.createSession('ni');
s.addAnalogInputChannel('Dev3',13,'Voltage'); % add input channels
s.addAnalogInputChannel('Dev3',14,'Voltage'); % add input channels
s.addAnalogInputChannel('Dev3',9,'Voltage'); % add input channels
s.DurationInSeconds=d.seconds; % [s] time for recording
s.Rate=d.fs; % set output and measuring frequency [Hz]

    %% acquire data
    d.hitInd=zeros([d.numlocs d.numhits]);
    pause(2) % provide time for user to move from computer to test station
        for iii=1:d.numlocs
            fprintf('Move to location %i\n', iii);
            % sound
            asdf=linspace(1/8192,1/4,2048);sound([sin(2*pi*1000*asdf)
sin(2*pi*800*asdf)],8192); % signals user to move on to next location

            pause(1) % pause allows user to move to new location
            jjj=1;
            while jjj<=d.numhits
                % sound
                asdf=linspace(1/8192,1/4,2048);sound(sin(2*pi*800*asdf),8192)
% signals user to hit immediately

                data_ind=jjj+(iii-1)*d.numhits; % integer increasing index to
append data to after data acquisition

                % data acquisition
                [d.data,d.time]=s.startForeground; % collect data for one
impact

                d.data_store(:,data_ind,:)=d.data; % append data to stored
matrix
                d.time_series(:,data_ind)=d.time; % append timeseries to
stored matrix
```

```
                hitIndCheck=find(abs(d.ch_sens(1).*d.data(1:end-
d.time_fft*d.fs,1))>d.threshold_impact_force,1,'first'); % check if impact
occurred with enough data after impact for processing
                if isempty(hitIndCheck)
                    % do nothing, repeat this iteration through the loop
                else
                    d.hitInd(iii,jjj)=hitIndCheck; % if hit did occur, append
to stored matrix
                    jjj=jjj+1;% if hit did occur, increase counter
                end
                % clear data for next loop
%                 d.data=[];
%                 d.time=[];
                hitIndCheck=[]; % clear data for next loop
            end
        end
%         fprintf('move laser to next location\n')
        % sound
        asdf=linspace(1/8192,1/4,2048);sound([sin(2*pi*1200*asdf)
sin(2*pi*1000*asdf)],8192); % signals user to move on to next location

%         pause % pause until user input to allow for laser to be moved
%         pause(1)
end
%% take FFT of data
samples_ahead=round(d.fs*d.time_fft); % # of samples to grab from impact time
to compute fft
nft=2^nextpow2(2*samples_ahead);
d.f_ft=d.fs/2*linspace(0,1,nft/2+1)'; % define frequency vector
window_hold=exp(-4*[1:samples_ahead]'/d.fs); % make exponential window to
scale the impact-induced displacement ring-down data
%window_hold=exp(-4*[1:138609]'/d.fs);
% exponential window recommended by
Avitable_experimental_modal_analysis_simple_non_mathematical_presentation
Sound and Vibration January 2001

%%
d.tf=[];d.tf_meanoutput=[];d.tf_meansq=[];d.tf_mean=[];data_ft=[];tf_data_on_
force=[];data_here=[];
    for iii=1:d.numlocs
        for jjj=1:d.numhits
            %%
            data_ind=jjj+(iii-1)*d.numhits; % index to retrieve collected
data from

            %% filter data
            ch_f=filtfilt(myfilt,d.data_store(:,data_ind,:)); %

            %%
            temp_ind_1=find(ch_f(d.hitInd(iii,jjj)-
round(d.fs*d.sec_jump):d.hitInd(iii,jjj),1)<0,1,'last')+d.hitInd(iii,jjj)-
round(d.fs*d.sec_jump); % find the start of the impulse peak (voltage crosses
0)

temp_ind_2=find(ch_f(d.hitInd(iii,jjj):d.hitInd(iii,jjj)+round(d.fs*d.sec_jum
```

```
p),1)<0,1,'first')+d.hitInd(iii,jjj); % find the end of the impulse peak
(voltage crosses 0)
            d.force_amplitude(iii,jjj)=max(d.ch_sens(1)*ch_f(:,1)); % find
amplitude of force
            d.output_amplitude(iii,jjj,1)=max(d.ch_sens(2)*ch_f(:,2)); % find
amplitude of output
            d.output_amplitude(iii,jjj,2)=max(d.ch_sens(3)*ch_f(:,3)); % find
amplitude of output
            for zzz=1:d.numoutputs

data_here(:,zzz)=d.ch_sens(zzz+1).*ch_f(temp_ind_1:temp_ind_1+samples_ahead-
1,zzz+1); % current evaluation of force data
%                 figure(23);
%                 clf;
%                 plot(accel_here(:,zzz));
%                 drawnow

% compute decay rate of impulse response from exponential fit of amplitude
peaks
atrunc=1:round(.025*length(data_here(:,zzz)));
[holding1,holdind1]=findpeaks(abs(data_here(atrunc,zzz))); % finding peaks
from abs data
temptime=[1:length(data_here(atrunc,zzz))]/d.fs; % create dummy time series
temp_fit=fit(temptime(holdind1)',holding1,'exp1');
%figure(1);clf;box
on;plot(temptime(holdind1)',holding1,'or',temptime(holdind1)',temp_fit.a.*exp
(temp_fit.b*temptime(holdind1)'),'-b');set(gca,'yscale','log');axis([0 .002
1e-2 100]);drawnow
d.decay_rate(iii,jjj,zzz)=temp_fit.b;

                data_mean_here(zzz)=mean(data_here(:,zzz)); % mean of
start/stop data in this time frame
                data_ft(:,zzz)=fft((data_here(:,zzz)-
data_mean_here(zzz)).*window_hold,nft)/(samples_ahead*mean(window_hold)); %
impact fft on disp, take fast fourier transform of exponentially windowed
data
                %data_ft(:,zzz)=fft((data_here(:,zzz)-
data_mean_here(zzz)).*window_hold,nft)/(length(data_here)*mean(window_hold));
% impact fft on disp, take fast fourier transform of exponentially windowed
data


tf_data_on_force(:,zzz)=data_ft(:,zzz)./d.force_amplitude(iii,jjj);
                d.tf(:,iii,jjj,zzz)=tf_data_on_force(1:nft/2+1,zzz); % impact
fft on tf, magnitude of single-sided fourier transform
            end

            d.tf_meanoutput(:,iii,jjj)=mean(squeeze(d.tf(:,iii,jjj,:)),2); %
take mean across number of simultaneous outputs)

%             figure(23);
%             clf;
%             plot(d.f_ft,abs(d.tf_meanoutput(:,iii,jjj)));
%             xlim([50 2e3]);
%             drawnow
```

```
        end
        d.tf_mean(:,iii)=mean(squeeze(d.tf_meanoutput(:,iii,:)),2); % take
mean across hits at location iii
        %     d.tf=[];
    end
    d.tf_meansq=mean(d.tf_mean.^2,2); % take mean across all locations

%%
d.tf_global_mean=(d.tf_meansq).^(1/2); % take mean across laser locations for
global response
d.tf_global_mean_amplitude=2*abs(d.tf_global_mean); % take abs of global mean
for plotting purposes

%% plot TF
% figure(8);
% clf;
% % hold on
% loglog(d.f_ft,d.tf_global_mean_amplitude);
% xlabel('frequency [Hz]')
% ylabel('TF, data/impact force [unit/N]')
% xlim([50 20000])
% title({[d.filename] ['global response of displacement on force']
[num2str(d.numlocs) ' input locs with ' num2str(d.numhits) ' hits each and '
num2str(d.numoutputs) ' output locs']},'Interpreter','none')
% figname=d.filename(1:end-4);
% % saveas(gcf,figname,'fig')

%% save data
if saveon==1 && dataacquire==1
    % remove data time series for memory-saving
%     d.time=[];
%     d.data=[];
%     d.time_series=[];
%     d.data_store=[];
    d.tf=[];
    d.tf_meanoutput=[];

    save(d.filename,'d');
end

%%
%% plot octave or one-third octave band measures
ob=1e3*2.^[-6:4]; % octave band center frequencies [Hz]
ob_lo=ob./2.^(1/2); % octave band center frequency lower [Hz]
ob_hi=ob.*2.^(1/2); % octave band center frequency higher [hz]
otob=1e3*2.^([-18:12]/3); % one-third octave band center frequencies [Hz]
otob_lo=otob./2.^(1/6); % one-third octave center frequency lower [Hz]
otob_hi=otob.*2.^(1/6); % one-third octave center frequency lower [Hz]

% determine octave and one-third octave band measures
% octave band
for jjj=1:length(ob)
ind1=max(find(d.f_ft<=ob_lo(jjj)));
ind2=max(find(d.f_ft<=ob_hi(jjj)));
tf_ob(jjj)=(sum(d.tf_global_mean_amplitude(ind1:ind2).^2)).^(1/2);
end
```

```
% one-third octave band
for jjj=1:length(otob)
ind1=max(find(d.f_ft<=otob_lo(jjj)));
ind2=max(find(d.f_ft<=otob_hi(jjj)));
tf_otob(jjj)=(sum(d.tf_global_mean_amplitude(ind1:ind2).^2)).^(1/2);
end

colors=['r' 'g' 'b' 'c' 'm' 'k'];
markers=['o' 's' 'd' 'v' '^' '*'];
color_plot=1;

figure(3);
clf;
hold on
box on
% plot(d.f_ft,d.tf_global_mean_amplitude);
plot(d.f_ft,10*log10(d.tf_global_mean_amplitude),'color',colors(color_plot));
xlabel('frequency [Hz]')
ylabel('TF, response/(impact force) [dB re 1 unit/N]')
set(gca,'xscale','log');
% set(gca,'yscale','log');
xlim([50 20000])
title({[strrep(d.filename,'_','-')] ['ratio of global response on force']
[num2str(d.numlocs) ' input locs with ' num2str(d.numhits) ' hits each and '
num2str(d.numoutputs) ' output locs']});
figure(4);
clf;
hold on
box on
% plot(otob,tf_otob,'-o');
plot(otob,10*log10(tf_otob),['-' colors(color_plot) markers(color_plot)]);
xlabel('frequency [Hz]');
ylabel({['1/3-octave band TF'],['response/(impact force) [dB re 1
unit/N]']});
set(gca,'xscale','log');
% set(gca,'yscale','log');
xlim([50 20000]);
title({[strrep(d.filename,'_','-')] ['ratio of global response on force']
[num2str(d.numlocs) ' input locs with ' num2str(d.numhits) ' hits each and '
num2str(d.numoutputs) ' output locs']});

% compute octave band total measures
% disp([num2str(10*log10(sum(tf_ob(3:end))),'%1.3f') ' [dB] from 62.5 to 16e3
[Hz] octave bands. ' d.filename]);
% disp([num2str(10*log10(sum(tf_ob(3:8))),'%1.3f') ' [dB] from 62.5 to 2e3
[Hz] octave bands. ' d.filename]);
% disp([num2str(10*log10(sum(tf_ob(3:7))),'%1.3f') ' [dB] from 62.5 to 1e3
[Hz] octave bands. ' d.filename]);
d.data_temp_hold(1)=10*log10(sum(tf_ob(4:end))); % store octave band 125 to
16e3 TF
d.data_temp_hold(2)=10*log10(sum(tf_ob(4:8))); % store octave band 125 to 2e3
TF
d.data_temp_hold(3)=10*log10(sum(tf_ob(4:7))); % store octave band 125 to 1e3
TF
%%
%plotting decay rate v force amplitude
```

```
figure(985);
%clf;
decay_rate=[d.decay_rate(:,1)',d.decay_rate(:,2)'];
% mean=mean(decay_rate)
% std=std(decay_rate)
plot(d.force_amplitude,squeeze(d.decay_rate),'^','Color','b');
hold on
xlabel('force (N)');
ylabel('decay rate');
title({[strrep(d.filename,'_','-')] ['decay rate v force']
[num2str(d.numlocs) ' input locs with ' num2str(d.numhits) ' hits each and '
num2str(d.numoutputs) ' output locs']});
%%
%plotting output amplitude max v force amplitude max
figure(984);
%clf;
plot(d.force_amplitude,squeeze(d.output_amplitude),'^','Color','b');
xlabel('force [N]');
ylabel('amplitude of output [m/s^2]');
title({[strrep(d.filename,'_','-')] ['decay rate v force']
[num2str(d.numlocs) ' input locs with ' num2str(d.numhits) ' hits each and '
num2str(d.numoutputs) ' output locs']});
hold on
%% plotting time series data
time_series_set=9;
figure(7);
clf
hold on
%
plot(d.time_series(:,time_series_set),d.data_store(:,time_series_set,1)*d.ch_
sens(1),d.time_series(:,time_series_set),d.data_store(:,time_series_set,2)*d.
ch_sens(2));
%
plot(d.time_series(:,time_series_set),d.data_store(:,time_series_set,2)*d.ch_
sens(2));
plot(d.time_series(:,time_series_set),d.data_store(:,time_series_set,1)*d.ch_
sens(1),d.time_series(:,time_series_set),d.data_store(:,time_series_set,2)*d.
ch_sens(2),d.time_series(:,time_series_set),d.data_store(:,time_series_set,3)
*d.ch_sens(3));
xlabel('Time (s)');
ylabel('Amplitude');
title({[strrep(d.filename,'_','-')] ['time series'] [num2str(d.numlocs) '
input locs with ' num2str(d.numhits) ' hits each and ' num2str(d.numoutputs)
' output locs']});
legend('Force','Accel1','Accel2')
%%
% colors=['r' 'g' 'b' 'c' 'm'];
% hit_sequence=13;
%
myfilt1=designfilt('bandpassiir','filterorder',12,'HalfPowerFrequency1',d.fil
ter_data_lo,'HalfPowerFrequency2',d.filter_data_hi,'samplerate',d.fs); %
filter result
%
myfilt2=designfilt('bandpassiir','filterorder',12,'HalfPowerFrequency1',5e2,'
HalfPowerFrequency2',d.filter_data_hi,'samplerate',d.fs); % filter result
% figure(2);
% clf;
```

```
% hold on;
% for ooo=1:2,
% %     if ooo==1
% %
plot_data=filtfilt(myfilt1,d.ch_sens(ooo)*squeeze(d.data_store(:,hit_sequence
,ooo)));
% %     else
% %
plot_data=filtfilt(myfilt2,d.ch_sens(ooo)*squeeze(d.data_store(:,hit_sequence
,ooo)));
% %     end
%     plot_data=d.ch_sens(ooo)*squeeze(d.data_store(:,hit_sequence,ooo));
%     plot(d.time_series(:,hit_sequence),plot_data,'color',colors(ooo));
% end;
% xlabel('time [s]');
% ylabel('force [N], acceleration [m/s2]');
% title({[strrep(d.filename,'_','-')] ['impact sequence '
num2str(hit_sequence) ] ['r g b c m. force-1, accel-2:5']});
```

6.1.3 Acquisition Code for Shaker Transducer Test

```
%% data acquisition toolbox NI
clear all
warning off

%%
% preset post-processing built for constant-frequency & frequency-sweep
% experiments, for random experiments, and for ring-down experiments.

% the excitation parameters are not defined here, because they are presumed
% to either be nill (for 'ring-down') or governed by the vibration controller
% such as the Vibration Research VR9500

% thus, if using the controller for excitation purposes, the input
% parameters for the controller are determined via the post-processing
% here and the first channel is presumed to be the control accelerometer.

% for 'ring-down' type experiments, one must correctly identify the
% associated input channels with the responses of interest

%% acquire data?
dataacquire=1; % yes for acquire

%% post-processing relevant parameters
% test types are:
% 'sine' which is either frequency sweep or constant-frequency sinusoid
% 'random' which is random excitation
% 'ring-down' which are impulses on test components, used to determine
natural frequencies and damping ratios
% NOTE: each test may require a modified hi and lo frequency cutoff set for
the digital filtering
d.test_type='random'; %!!!!!!

%% test specimen name
d.specimen='Control'; % specimen name, or no_specimen if none!!!!!!!!

%% data acquisition setup parameters
d.fs=131072; % sampling frequency [Hz]
d.wind=@hann; % window type for averages
d.seconds=60; % [s] seconds of data acquisition!!!!!!!, determined according
to Vibration Research VR9500 controller test setup
d.filter_data_lo=500; % [Hz] of low pass cut off frequency
d.filter_data_hi=20e3; % [Hz] of high pass cut off frequency!!!!!!!!!!

%% fft computation parameters
% for 'sine' and 'random' tests only
% TIME_SAMPLED_PER_FFT is very important towards quality of post-processed
% data. If first attempt is not so great, try greater and lesser values.
d.time_sampled_per_fft=2; % [s] seconds of data acquisition over which fft is
evaluated
d.spacing_cts=round(d.fs*d.time_sampled_per_fft); % number of samples to use
in FFT to obtain freq_spacing
d.fft_numbers=floor(d.fs*d.seconds/d.spacing_cts); % number of ffts to
compute/loop through
```

```
d.nft=2^nextpow2(d.spacing_cts); % number of samples next to power of 2 for
spacing_cts

%% filename for save d structure
c=clock; % grab the time-stamp, eliminates possibility of data overwrite
d.filename=[num2str(c(1)) '_' num2str(c(2),'%02.0f') '_'
num2str(c(3),'%02.0f') '_' num2str(c(4),'%02.0f') num2str(c(5),'%02.0f') '_'
d.test_type '_' d.specimen '.mat'];
saveon=1; % save the data?

%% sensor sensitivity
d.sensor{1}='PCB_208C01_SN_LW43812_force_transducer_input_from_shaker';
d.sensor{2}='PCB_352A24_SN_LW211073_accelerometer_on_specimen';
d.ch_sens(1)=1/.1125; % N/V  % PCB_208C02 force transducer
d.ch_sens(2)=1/.01022; % (m/s^2)/V % PCB_U352A10 accelerometer

%% mean sensor values [V] for each channel, to be subtracted from the input
before sensitivity to [units]
d.data_mean(1)=0; %
d.data_mean(2)=0; %

%% if for data acquisition
if dataacquire==1 % 1=yes for acquire

%% identify connected devices
devices=daq.getDevices;
% once obtained, ensure using correct device name in below session and
acquire lines

%% acquire data
s=daq.createSession('ni');
s.addAnalogInputChannel('Dev3',6,'Voltage'); % add input channels
s.addAnalogInputChannel('Dev3',10,'Voltage');
s.Rate=d.fs; % set output and measuring frequency [Hz]
s.DurationInSeconds=d.seconds; % [s] duration of data acquisition
[d.data,d.time_series]=s.startForeground;
d.nn_chan=min(size(d.data));

%% bandpass filter data
clear ch_f
d.nn_chan=min(size(d.data));
%
myfilt=designfilt('lowpassiir','filterorder',4,'passbandfrequency',d.filter_d
ata_hi,'PassbandRipple',0.01,'samplerate',d.fs);
myfilt=designfilt('bandpassiir','filterorder',4,'HalfPowerFrequency1',d.filte
r_data_lo,'HalfPowerFrequency2',d.filter_data_hi,'samplerate',d.fs);
for iii=1:d.nn_chan
ch_f(:,iii)=filtfilt(myfilt,d.ch_sens(iii)*(d.data(:,iii)-d.data_mean(iii)));
%
end
%%
end
%%
d.data_filt=ch_f; % re-assign filtered data from local to structure variable
%% post-process data
```

```
%%
if strcmp(d.test_type,'sine')==1
%%
clear ch_ft gxy gxx coh tf y
d.inst_mean=[];d.f_ft=[];d.meansq=[];d.corr=[];d.lags=[];d.ch_ft_instavg=[];d
.freq_instavg=[];d.tf_est_instavg=[];d.gxx_instavg=[];d.gxy_instavg=[];
for ooo=1:2*d.fft_numbers-1 %  1:d.fft_numbers for no overlap.
1:2*d.fft_numbers-1 with half-overlap as defined below in trunc
    %     trunc=(ooo-1)*d.spacing_cts+1:ooo*d.spacing_cts; % define
truncation in time : no overlap in averaging
    trunc=(ooo-1)*d.spacing_cts/2+1:ooo*d.spacing_cts/2+d.spacing_cts/2; %
define truncation in time : gives half-overlap of windowed averages is the
ooo=1:2*d.fft_numbers-1
    for iii=1:d.nn_chan
    d.inst_mean(ooo,iii)=mean(d.data_filt(trunc,iii)); % mean of
instantaneous data stream for the channel

y(:,iii)=fft(d.data_filt(trunc,iii).*window(d.wind,length(trunc)),d.nft)/(d.s
pacing_cts*mean(window(d.wind,length(trunc))));
%     y(:,iii)=fft(d.data_filt(trunc,iii),d.nft)/(d.spacing_cts); % take fast
fourier transform of data
    ch_ft(:,iii,ooo)=2*abs(y(1:d.nft/2+1,iii)); % magnitude of single-sided
fourier transform
    d.f_ft=d.fs/2*linspace(0,1,d.nft/2+1)'; % define frequency vector
    gxx(:,iii,ooo)=y(:,iii).*conj(y(:,iii))/2; % auto power spectrum
    if iii>0
    gxy(:,iii,ooo)=y(:,iii).*conj(y(:,1))/2; % cross power spectrum,
referencing input force
    end
    if iii>2

tf_est(:,iii,ooo)=tfestimate(d.data_filt(trunc,2),d.data_filt(trunc,iii),[],[
],d.nft,d.fs); % transfer function estimate
    end

    d.meansq(iii,ooo)=mean((d.data_filt(trunc,iii)-d.inst_mean(ooo,iii)).^2);
% mean-square system response [units]^2, with mean eliminated
    [d.corr(:,iii,ooo),d.lags]=xcorr(d.data_filt(trunc,iii)-
d.inst_mean(ooo,iii),d.data_filt(trunc,iii)-d.inst_mean(ooo,iii),'unbiased');
% autocorrelation of the signal
    end

%     figure(23);clf;plot(d.f_ft,squeeze(ch_ft(:,1,ooo)));xlim([5
250]);xlabel('frequency [Hz]');ylabel('control accel [m/s2]');drawnow;

    [mmx,ind]=max(squeeze(ch_ft(5:end,1,ooo))); % grab max and location of
max for first channel, control accelerometer, to identify the instantaneous
frequency [Hz]
    % the above look forward by 4 indices is to eliminate potential for high
DC component (due to signal shift) which will mislead results
    ind=ind+4; % look forward to accommodate above processing
    d.freq_instavg(ooo)=d.f_ft(ind); % [Hz] mean instantaneous excitation
frequency
    d.ch_ft_instavg(ooo,:)=max(squeeze(ch_ft(ind-2:ind+2,:,ooo)),[],1); % the
signals' FFT amplitude at this instantaneous frequency [units]
```

```
    d.gxx_instavg(ooo,:)=max(squeeze(gxx(ind-2:ind+2,:,ooo)),[],1); % the
signals' autospectral density at this instantaneous frequency [units^2]
    d.gxy_instavg(ooo,:)=max(squeeze(gxy(ind-2:ind+2,:,ooo)),[],1); % the
signals' cross spectral density at this instantaneous frequency [units^2]
    d.tf_est_instavg(ooo,:)=max(squeeze(tf_est(ind-2:ind+2,:,ooo)),[],1); %
the signals' transfer function at this instantaneous frequency [units^2]

    indt=ind; % hold index

end
%%
close 23
%% plot
figure(2);
% clf;
hold on;
plot(d.freq_instavg,abs(d.tf_est_instavg(:,2)),'o')
%
plot(d.freq_instavg,real(d.tf_est_instavg(:,3)),'o',d.freq_instavg,imag(d.tf_
est_instavg(:,3)),'s')
xlabel('frequency [Hz]');
ylabel('transfer function, output force / input force [dim]');
set(gca,'yscale','log')
box on

%%
end
%%
%%
if strcmp(d.test_type,'random')==1
%%
clear ch_ft gxy gxx coh tf y
d.inst_mean=[];d.f_ft=[];d.ch_ft_a=[];d.gxx_a=[];d.gxy_a=[];d.tf_est_a=[];
for ooo=1:2*d.fft_numbers-1 %  1:d.fft_numbers for no overlap.
1:2*d.fft_numbers-1 with half-overlap as defined below in trunc
%     trunc=(ooo-1)*d.spacing_cts+1:ooo*d.spacing_cts; % define truncation in
time : no overlap in averaging
    trunc=(ooo-1)*d.spacing_cts/2+1:ooo*d.spacing_cts/2+d.spacing_cts/2; %
define truncation in time : gives half-overlap of windowed averages is the
ooo=1:2*d.fft_numbers-1
    for iii=1:d.nn_chan
    d.inst_mean(ooo,iii)=mean(d.data_filt(trunc,iii)); % mean of
instantaneous data stream for the channel

y(:,iii)=fft(d.data_filt(trunc,iii).*window(d.wind,length(trunc)),d.nft)/(d.s
pacing_cts*mean(window(d.wind,length(trunc))));
    ch_ft(:,iii,ooo)=2*abs(y(1:d.nft/2+1,iii)); % magnitude of single-sided
fourier transform
    d.f_ft=d.fs/2*linspace(0,1,d.nft/2+1)'; % define frequency vector
    gxx(:,iii,ooo)=y(:,iii).*conj(y(:,iii))/2; % auto power spectrum
    if iii>1
    gxy(:,iii,ooo)=y(:,2).*conj(y(:,iii))/2; % cross power spectrum,
referencing input force
    end
    if iii>1
```

```
tf_est(:,iii,ooo)=tfestimate(d.data_filt(trunc,1),d.data_filt(trunc,iii),[],[
],d.nft,d.fs); % transfer function estimate
    end
    end


figure(23);clf;semilogy(d.f_ft,squeeze(ch_ft(:,1,ooo)));xlim([d.filter_data_l
o d.filter_data_hi]);xlabel('frequency [Hz]');ylabel('input [N]');drawnow;

end

for iii=1:d.nn_chan
d.ch_ft_a(:,iii)=mean(squeeze(ch_ft(1:d.nft/2+1,iii,:)),2); % average fft of
signal
d.gxx_a(:,iii)=mean(squeeze(gxx(1:d.nft/2+1,iii,:)),2); % average
autospectrum of signal
d.gxy_a(:,iii)=mean(squeeze(gxy(1:d.nft/2+1,iii,:)),2); % average
crosspectrum of signal
d.tf_est_a(:,iii)=mean(squeeze(tf_est(1:d.nft/2+1,iii,:)),2); % average
transfer functions
end

%%
% close 23
%% plot

colors=['r' 'g' 'b' 'c' 'm'];
markers=['o' 's' 'd' 'v' '^'];
color_plot=3; % color for this plot

figure(2);
clf;
% hold on;
semilogy(d.f_ft,10*log10(abs(d.tf_est_a(:,2))),'color',colors(color_plot));
% semilogy(d.f_ft,10*log10(abs(d.ch_ft_a(:,2))),'color',colors(color_plot));
xlabel('frequency [Hz]');
xlim([d.filter_data_lo d.filter_data_hi]);
% ylim([-40 10]);
box on
ylabel('transfer function, output acceleration / input force [dB re:1.0
(m/s^2)/N]');
% set(gca,'xscale','log')
set(gca,'yscale','linear');
title({[strrep(d.filename,'_','-')]});
% savefig([strrep(d.filename,'_','-') '_narrowband.fig']);

ob=1e3*2.^[-6:4]; % octave band center frequencies [Hz]
ob_lo=ob./2.^(1/2); % octave band center frequency lower [Hz]
ob_hi=ob.*2.^(1/2); % octave band center frequency higher [hz]
otob=1e3*2.^([-18:14]/3); % one-third octave band center frequencies [Hz]
otob_lo=otob./2.^(1/6); % one-third octave center frequency lower [Hz]
otob_hi=otob.*2.^(1/6); % one-third octave center frequency higer [Hz]

% determine octave and one-third octave band force transmissibility
```

```
% octave band
for jjj=1:length(ob)
ind1=max(find(d.f_ft<=ob_lo(jjj)));
ind2=max(find(d.f_ft<=ob_hi(jjj)));
tf_ob(jjj)=sum(abs(d.tf_est_a(ind1:ind2,2)).^2);
end
% one-third octave band
for jjj=1:length(otob)
ind1=max(find(d.f_ft<=otob_lo(jjj)));
ind2=max(find(d.f_ft<=otob_hi(jjj)));
tf_otob(jjj)=sum(abs(d.tf_est_a(ind1:ind2,2)).^2);
end

%
figure(222);
clf;
hold on;
box on
semilogy(otob,10*log10(tf_otob.^(1/2)),['-' markers(color_plot)
colors(color_plot)]);
xlim([d.filter_data_lo d.filter_data_hi]);
% ylim([-35 10]);
set(gca,'xscale','log');
set(gca,'yscale','linear');
xlabel('frequency [Hz]');
ylabel('1/3-octave band transfer function, output acceleration / input force
[dB re:1.0 (m/s^2)/N]');
% set(gca,'xminortick',xmt);
title({[strrep(d.filename,'_','-')]});
% savefig([strrep(d.filename,'_','-') '_otob.fig']);

%% cumulative octave band
disp([num2str(10*log10(sum(tf_otob(22:29)).^(1/2)),'%1.4f') ' [dB] from 2e3
to 10e3 [Hz] 1/3-octave bands. ' d.filename]);
data_temp_hold(color_plot,1)=10*log10(sum(tf_otob(22:29)).^(1/2)); % store
1/3-octave band 2e3 to 10e3 TFclear

disp([num2str(10*log10(sum(tf_otob(30:32)).^(1/2)),'%1.4f') ' [dB] from
12.5e3 to 20e3 [Hz] 1/3-octave bands. ' d.filename]);
data_temp_hold(color_plot,2)=10*log10(sum(tf_otob(30:32)).^(1/2)); % store
1/3-octave band 12.5e3 to 20e3 TFclear

% disp([num2str(10*log10(sum(tf_otob(16:19)).^(1/2)),'%1.4f') ' [dB] from 500
to 1e3 [Hz] 1/3-octave bands. ' d.filename]);
% data_temp_hold(color_plot,3)=10*log10(sum(tf_otob(16:19)).^(1/2)); % store
1/3-octave band 500 to 1e3 TFclear

% disp([num2str(10*log10(sum(tf_otob(7:13)).^(1/2)),'%1.4f') ' [dB] from 62.5
to 250 [Hz] 1/3-octave bands. ' d.filename]);
% data_temp_hold(color_plot,3)=10*log10(sum(tf_otob(7:13)).^(1/2)); % store
1/3-octave band 62.5 to 250 TFclear
%%
end
```

```
%%
%%
if strcmp(d.test_type,'ring-down')==1
%%
clear ch_ft gxy gxx coh tf y
% identify start and stop times
ind1=max(find(d.time_series<=14.6));
ind2=max(find(d.time_series<=15));
trunc=ind1:ind2;
d.nft=2^nextpow2(length(trunc)); % number of samples next to power of 2 for
spacing_cts
for iii=1:d.nn_chan

y(:,iii)=fft(d.data_filt(trunc,iii).*window(d.wind,length(trunc)),d.nft)/(len
gth(trunc)*mean(window(d.wind,length(trunc))));
    ch_ft(:,iii)=2*abs(y(1:d.nft/2+1,iii)); % magnitude of single-sided
fourier transform
    d.f_ft=d.fs/2*linspace(0,1,d.nft/2+1)'; % define frequency vector
end
d.f_ft=d.fs/2*linspace(0,1,d.nft/2+1)'; % define frequency vector
figure(23);
clf;
semilogy(d.f_ft,ch_ft(:,3))
xlabel('frequency [Hz]');
ylabel('fft [units]');
xlim([5 100]);

%%
%% plot

%%
end

%%

%% save data
if saveon==1
    d.data_filt=[];
    d.data=[];
    d.time_series=[];
    d.inst_mean=[];
    d.meansq=[];
    d.corr=[];
    d.lags=[];
    save(d.filename,'d');
end

%%

%%
```